Tropical tropospheric ozone and carbon monoxide distributions: characteristics, origins and control factors, as seen by IAGOS and IASI

Maria Tsivlidou[1], Bastien Sauvage[1], Yasmine Bennouna[1], Romain Blot[1], Damien Boulanger[2], Hannah Clark[3], Eric Le Flochmoën[1], Philippe Nédélec[1], Valérie Thouret[1], Pawel Wolff[2], and Brice Barret[1]

[1]Laboratoire d'Aérologie (LAERO), Université Toulouse III – Paul Sabatier, CNRS, Toulouse, France
[2]Observatoire Midi-Pyrénées (OMP-SEDOO), Université Toulouse III - Paul Sabatier, CNRS, Toulouse, France
[3]IAGOS-AISBL, 98 Rue du Trône, Brussels, Belgium

Correspondence: Maria Tsivlidou (mtsivl@gmail.com)

Abstract. The characteristics and seasonal variability of the tropical tropospheric distributions of ozone (O_3) and carbon monoxide (CO) were analysed based on in situ measurements provided by the In-service Aircraft for a Global Observing System (IAGOS) program since 1994 and 2002 respectively, combined with observations from the Infrared Atmospheric Sounding (IASI) instrument on board the Met-op A satellite since 2008. The SOFT-IO model, which couples back trajectories with CO emissions inventories, was used to explore the origins and sources of the tropical CO observed by IAGOS. The highest tropical O_3 and CO maxima occur over Northern Tropical (NT) Africa in the low troposphere (LT; surface to 750 hPa) during the dry season (75 ppb of O_3 at 2.5 km and 850 ppb of CO at 0.3 km over Lagos in January). Despite the active local fires, local anthropogenic (AN) emissions (58 %) are dominant for the CO. The importance of the local AN emissions are highlighted over Central Africa, as they cause a persistent polluted surface layer during the transition seasons (40 % in October and 86 % in April). The second highest O_3 and CO maxima are observed over Asia. Local or regional Asian AN emissions cause the CO maximum in the LT (at 0.5 km) in January, and the O_3 maximum in above 6 km in the post-monsoon season (April). South China is the only Asian site where O_3 peaks in the LT (75 ppb at 2.5 km), due to local fires (30 %) in addition to the local (52 %) and regional (15 %) AN emissions. The highest amount of transported CO originates from Africa. The main transport pathway is from the dry-season African regions towards the wet-season ones. Contributions from Northern Hemisphere Africa are found over Arabia and Eastern Africa (up to 70 %) during the dry season and over South America all year long in the mid (MT; 750–300 hPa) and upper troposphere (UT; 300–200 hPa)(18–38 % over Caracas on annual basis). In contrast, the impact of the Asian emissions in the LT and MT is limited on a local or regional scale. Export of polluted Asian air masses is important in the UT during the Asian summer monsoon and post-monsoon seasons, when convection is active. The AN Asian contributions are mostly found over Arabia and Eastern Africa (up to 80 %) during the Asian summer monsoon. During the post-monsoon, CO impacted by the Indonesian fires (resp. SouthEast Asian AN emissions) are transported towards Eastern Africa (64% and 16%) due to the Tropical Easterly Jet. The lowest O_3 and CO levels are observed over South America, due to less strong local emissions in comparison to Asia and Africa. The only important CO and O_3 enhancement is observed in

the MT during the local fires (October), when O_3 and precursors impacted by the local AN and fire emissions are trapped in an anticyclone and transported towards Southern Africa (5–10 ppb from Northern and Southern Hemisphere South America respectively).

1 Introduction

Tropospheric ozone (O_3) and carbon monoxide (CO) are key components in the atmosphere. O_3 has a significant impact on human health close to the surface (Curtis et al., 2006; Jerrett et al., 2009) and on climate by being a powerful greenhouse gas (Gauss et al., 2003; IPCC, 2021). O_3 is a secondary pollutant produced by photochemical oxidation of precursors such as CO and volatile organic compounds (VOCs) in the presence of nitrogen oxides (NO_x) (Logan et al., 1981). Its distribution is controlled by: stratospheric transport (Stevenson et al., 2013); transport processes at intercontinental and hemispheric scale (Wild et al., 2004); emissions of precursors (natural and anthropogenic) and destruction processes (photochemical and depositional) (Monks et al., 2015). Due to its longer lifetime, CO is considered a powerful pollution tracer of combustion products at a hemispheric level (Logan et al., 1981). CO impacts the oxidation capacity of the atmosphere by being the major sink of OH radicals in non polluted atmosphere (Lelieveld et al., 2016), and the climate by producing greenhouse gases, such as CO_2 and O_3, during its oxidation (Myhre et al., 2013). CO is primarily emitted by incomplete combustion, thus by anthropogenic (AN) and biomass burning (BB) sources (Galanter et al., 2000; Granier et al., 2011), with contributions between 450–600 and 350–600 Tg CO yr^{-1} respectively (Lamarque et al., 2010; van der Werf et al., 2006). Its secondary sources include oxidation of VOCs and methane (450–1200 and 600– 1000 Tg CO y^{-1} resp.; (Stein et al., 2014)).

Recent studies (Gaudel et al., 2018, 2020; Zhang et al., 2016) have shown increasing tropospheric O_3 burden in the second half of the 20th century mostly due to increase of precursors in the tropical regions. Based on aircraft observations, Bourgeois et al. (2020) recently presented a global-scale distribution of O_3 in the remote troposphere. However, uncertainties still remain in the global O_3 distribution and sources of precursors due to paucity of observations in the free troposphere, especially over developing countries in the tropics (Gaudel et al., 2018; Tarasick et al., 2019).

The tropical region is of particular interest regarding tropospheric O_3 and CO. It combines: i) intense photochemistry due to high UV radiation and humidity, ii) large active natural sources of CO and other O_3 precursors through BB (Ziemke et al., 2009), biogenic (Aghedo et al., 2007) and lighting emissions (Sauvage et al., 2007b, c), iii) increasing AN due to rapid industrialisation (Granier et al., 2011; Duncan et al., 2016), iv) large ozone net production potential because deep convection can transport surface emissions to higher altitudes, where their lifetime is increased due to lack of surface deposition and dilution with unpolluted background (Pickering et al., 1995) and v) dynamic processes capable of redistributing chemical species in a regional and global scale (Zhang et al., 2016). Thus, the tropics are a region where O_3 production is favoured.

Satellite observations from the OMI and MLS sensors (Ziemke et al., 2019) and simulations from the GEOS-Chem chemical transport model (Zhang et al., 2016, 2021) display the highest O_3 burden increase in the tropical region - mostly over India, East Asia and SouthEast Asia. Most studies tend to confirm an increase of O_3 in the tropics but they are mostly based on model simulations, sparse ground observations or satellite data with little consistency, and it is not clear what can cause such an increase. Indeed the trends are attributed to different factors such as BB (Heue et al., 2016), dynamics (Lu et al., 2019; Thompson et al., 2021), or AN (Zhang et al., 2016; Gaudel et al., 2020). Thus, further investigation based on *in situ* observations is required in order to better constraint models, validate satellite retrievals, and reduce the uncertainties in the quantification of O_3 and CO trends and source attribution over the tropics.

Measurements of tropical O_3 and CO are available by satellite observations, but they have a coarse vertical resolution (e.g. Barret et al., 2008; Thompson et al., 2001). On short time scales, several field campaigns have been carried out in the tropics, yielding measurements of various species over Africa (from TROPOZ 1987 to CAFE-Africa), Asia (from INDOEX to EMerge-Asia), South America (Cite-1/2/3, TROCCiNOX) and the tropical Pacific (from PEM-WEST-A/B to CAST/CONTRAST/ATTREX and Atom). These campaigns have provided invaluable insights on the atmospheric chemistry and dynamics of the tropical region. On greater timescales, the Southern Hemisphere ADditional OZone Sounding (SHADOZ) program (Thompson et al., 2003a) provides long-term O_3 observations over the tropics using ozonesondes since 1998. These measurements have offered a better understanding on the vertical distribution and trends of tropical O_3 (e.g. Thompson et al., 2021).

In a complementary way to these datasets, the IAGOS (In-service Aircraft for a Global Observing System; (Marenco et al., 1998; Petzold et al., 2015; Thouret et al., 2022) program has provided O_3 and CO measurements over the tropics since 1994 and 2002 respectively. Using equipped commercial aircraft, IAGOS samples vertical profiles at take off and landing, along with the lower part of the upper tropical troposphere at cruise altitude between 300 and 185 hPa (UT_{cruise}). Previous studies have documented the tropical composition over Africa (Sauvage et al., 2005, 2007a, d; Lannuque et al., 2021), South America (Yamasoe et al., 2015) and South Asia (Sahu et al., 2014; Sheel et al., 2014) using IAGOS data. However, they are focused on specific regions of the tropics and have limited temporal coverage, especially for CO as fewer measurements were available at this time. Thus, the O_3 and CO distributions and their interlocking in the entire tropics are still not well documented.

The SOFT-IO model (Sauvage et al., 2017) has been developed to supplement the analysis of the IAGOS dataset by estimating AN and BB contributions to the observed CO measurements. These measurements, along with the SOFT-IO output allow us to trace the CO origin over the tropics. Further, global distributions provided by Infrared Atmospheric Sounding Interferometer (IASI)-Software for a Fast Retrieval of IASI Data (SOFRID) (Barret et al., 2011; De Wachter et al., 2012) retrievals since 2008 complement the O_3 and CO distributions provided by IAGOS. They allow us to understand the spatial extent of pollution plumes, and explore intercontinental transport patterns.

In this article we take advantage of the unique IAGOS database to (i) document the characteristics and seasonal variability of these two atmospheric species over the whole tropical band for the last decade, (ii) explore the origin of the observed CO anomalies, (iii) investigate transport processes driving the CO and O_3 distribution in the tropics.

The observational (IAGOS and IASI) and model based (SOFT-IO) datasets, and methodology are introduced in Sect. 2. In Section 3, the IAGOS observations are analysed to document O_3/CO vertical profiles, along with the upper tropospheric composition over the tropics. In addition, the sources of observed CO are explored with SOFT-IO.

2 Data and Methods

2.1 IAGOS observations

The Research Infrastructure IAGOS (Petzold et al., 2015; Thouret et al., 2022) provides *in situ* measurements of trace gases (O_3, CO, water vapour, NO_y between 2001 and 2005 (e.g. Gressent et al., 2014), and more recently NO_x, CH_4, CO_2 and cloud particles, see https://www.iagos.org/iagos-data/) and meteorological parameters (temperature and winds), using equipped commercial aircraft. Full description of the instruments can be found in Nédélec et al. (2015). O_3 (resp. CO) is measured using a dual-beam ultraviolet absorption monitor (infrared analyser) with an overall uncertainty of ± 2 ppbv ± 2 % (± 5 ppbv ± 5 %) and a time resolution of 4 (resp. 30) seconds (Nédélec et al., 2015). IAGOS measures vertical profiles during ascend and descend phases, and the UT_{cruise} during cruise phases. Considering the aircraft speed (7–8 m s^{-1} during ascent/descent; 900 km h^{-1} during cruise), the time resolution of the instruments corresponds to a vertical resolution of 30 m (resp. 225 m), and a horizontal resolution of 1 km (resp. 7.5 km) for O_3 (resp. CO).

O_3 (resp. CO) observations have been collected since 1994 (resp. 2002) in the frame of the IAGOS Research Infrastructure and its predecessor MOZAIC (Marenco et al., 1998) program, based on the same instrument technologies. Good consistency in the measurements between the two programs (hereafter referred to as IAGOS) (Nédélec et al., 2015; Blot et al., 2021) leads to IAGOS temporal coverage of 26 (resp. almost 20) years for O_3 (resp. CO), depending on the availability of the flights. IAGOS data provides robust O_3 and CO climatologies, allowing studies of long-term trends (e.g. Cohen et al., 2018) along with validation of chemistry transport models (e.g. Sauvage et al., 2007b; Gressent et al., 2016) and satellite data retrievals (e.g. De Wachter et al., 2012) on a global scale. To complement the IAGOS observations, we use the potential vorticity (PV) field, which is part of the ancillary data (https://doi.org/10.25326/3) from the IAGOS database. The PV is calculated from the European Centre for Medium-Range Weather Forecast's (ECMWF) operational fields (horizontal resolution 1°, time resolution 3 hours), interpolated along IAGOS trajectories.

2.1.1 Data treatment

The tropical zone can be defined in several ways, such as by meteorological characteristics (e.g. location of the subtropical jets), climatic elements (e.g. precipitation rates) or by the geographical extent. Following the latter way, in the Tropospheric Ozone Assessment Report, Phase II (TOAR-II; https://igacproject.org/activities/TOAR/TOAR-II) Ozone and Precursors in the Tropics working group, the tropics are defined between 20° S and 20° N. In our study, we consider the extended area between 25° S and 25° N, in order to investigate interactions of pollution and the transport of air masses between the tropics and the subtropics. Only tropospheric measurements are taken into account, by applying a PV filter of 2 PV units (pvu) for

each measurement during cruise phase, and for the measurements between 20–25° N/S during ascend/descend. The UT_{cruise} climatologies are derived by averaging the cruise data on a 2 x 2.5° grid, for the period 1994–2020 (resp. 2002–2020) for O_3 (resp. CO). For the same time periods, the climatologies over the vertical are derived by averaging the data into 10 hPa pressure bins from the surface up to 200 hPa. We also applied a distance criteria of 300-km around the IAGOS observational site, similar to Petetin et al. (2016). This way we reduce uncertainties due to possible horizontal heterogeneity in the measurements, as the aircraft keeps moving in the horizontal plane during ascent and descent.

Table 1 shows the total number of profiles taken into account for this study for each site for the whole IAGOS period. The temporal availability of the measurements differ for each site and cluster, as it depends on the flight schedule of the aircraft (see Figs. S4 and S5). For this reason, to determine a reliable climatological profile, we need to assess the statistical significance of the data. Similar to Logan (1999) and Sauvage et al. (2005), we compute the relative standard error (RSE) of the O_3 (CO) monthly mean, versus the number of flights per month. The RSE is defined as the ratio between the standard error ($SE = \frac{\sigma}{\sqrt{N}}$, with σ the square root of the sample variance and N the number of flights) and the O_3 (CO) monthly mean. The minimum number of flights required for statistical significance corresponds to the number above which RSE $\leq$ 10 %. We choose RSE less than 10 %, because RSE depends not only on the number of measurements, but also on the O_3 (CO) variability which is high over the tropics (Thompson et al., 2003b). For each site with an adequate number of flights per month, we consider an individual profile of O_3 (CO). Otherwise, we combine sites in clusters, in order to increase the amount of data and get significant climatological profiles. Besides, the clusters can be useful for validation of models with a coarse horizontal resolution, because they represent a wider area as resolved by the models, which are not expected to capture small-scale variations in the ozone field (e.g. Emmons et al., 2010). For clustering, the sites should be: i) in relatively close distance from each other, ii) governed by similar meteorological conditions, and iii) display similar characteristics in the vertical distribution of O_3 (CO) (see Sect. 3.1).

The meteorological conditions in the tropics are peculiar, with different seasonal patterns depending on the region. For instance, in Africa the main seasons are two (dry and wet) with two intermediate seasons passing from wet to dry and vice versa (Sauvage et al., 2005; Lannuque et al., 2021). On the other hand, in Asia the seasons are defined by the Asian monsoon phases: Asian summer monsoon (wet season); Asian winter monsoon (dry season) and post monsoon. Thus, we considered it more appropriate for our analysis to deviate from the classical definition of the seasons, which fits better to studies concerning higher latitudes. Instead, we analyse the O_3/CO profiles and horizontal distributions for months during the peak tropical seasons (January, April, July and October), to highlight seasonal patterns.

2.2 SOFT-IO model

The SOFT-IO (SOft attribution using FlexparT and carbon monoxide emission inventories for In-situ Observation database) tool (Sauvage et al., 2017; http://dx.doi.org/10.25326/2) has been developed to investigate the origin of the observed IAGOS-CO, by coupling FLEXPART 20-days backward transport simulations with emission inventories. For each point of IAGOS trajectory, SOFT-IO estimates the CO contribution coming from 14 different geographical regions (see Fig. 1), for AN and BB origin separately. We use Community Emissions Data System (CEDS2) AN emissions (McDuffie et al., 2020) and the Global

Table 1. Description of individual sites and clusters used in this study. The location of the sites is displayed in Fig. 1. NT and ST indicate Northern and Southern Tropical Africa respectively. P O_3 and P CO indicate the total number of profiles for the IAGOS period.

	Individual sites/Clusters	IAGOS sites	P O_3	P CO
South America	South Brazil	Rio de Janeiro (Brazil), São Paulo (Brazil)	518	62
	Caracas	Caracas (Venezuela)	414	248
	Bogota	Bogota (Colombia)	190	142
NT Africa	Lagos	Lagos (Nigeria)	311	199
	Sahel	Abuja (Nigeria), Ouagadougou (Uganda), Niamey (Niger)	193	202
	Gulf of Guinea	Lome (Togo), Yaounde (Cameroon), Douala (Cameroon), Libreville (Gabon), Accra (Ghana), Abidjan (Ivory Coast), Malabo (Equatorial Guinea) Cotonou (Benin), Port Harcourt (Nigeria)	414	302
ST Africa	Central Africa	Luanda (Angola), Brazzaville (Congo) Kinshasa (Democratic Republic of Congo)	169	89
	Windhoek	Windhoek (Namibia)	651	692
Arabia and Eastern Africa	AbuDhabi	Abu Dhabi (United Arab Emirates), Muscat (Oman)	118	56
	Khartoum	Khartoum (Sudan)	157	116
	Addis Ababa	Addis Ababa (Ethiopia)	121	110
	Jeddah	Jeddah (Saudi Arabia)	154	108
Asia	South China	Hong Kong (China), Guangzhou (China), Xiamen (China)	337	562
	Gulf of Thailand	Kuala Lumpur (Malaysia), Singapore (Singapore)	162	140
	Madras	Madras (India)	239	253
	Hyderabad	Hyderabad (India)	159	170
	Mumbai	Mumbai (India)	61	29
	Manila	Manila (Philippines)	66	101
	Bangkok	Bangkok (Thailand)	526	336
	Ho Chi Minh City	Ho Chi Minh City (Vietnam)	113	90

Fire Assimilation System (GFAS) BB emissions (Kaiser et al., 2012) which include fire injection heights, to discriminate sources of CO anomalies over different regions of interest. For the calculations, the AN (resp. BB) emissions are updated on a monthly (resp. daily) basis.

SOFT-IO estimates the contribution to CO anomalies emitted by primary sources during the last 20 days, while it does not calculate the background CO. The background CO can be emitted by primary sources older than 20 days, and by secondary sources such as oxidation of methane and non-methane volatile organic compounds. The meteorological fields are based on 1° x 1° ECMWF analysis and forecast with a time resolution of 6 and 3h respectively.

Several studies (e.g. Cussac et al., 2020; Lannuque et al., 2021; Petetin et al., 2018b) have used SOFT-IO to track back the sources of CO measured by IAGOS. Sauvage et al. (2017) validated SOFT-IO performance against IAGOS CO observations for several regions and tropospheric levels. As detailed in their study, SOFT-IO uncertainties and biases are mostly due to uncertainties in emission inventories, and to a lesser extent to uncertainties concerning the meteorological fields and FLEXPART transport parameterizations (turbulence, convection). Their results show that SOFT-IO can simulate 95 % of the observed number of anomalies, without any strong dependence on altitude or region of the CO plume. SOFT-IO captures the intensity of CO anomalies with bias lower than 10-15 ppb for most of the regions and tropospheric levels. The bias is higher in extreme pollution events and might be related to uncertainties in the emissions inventories.

In our study, CO anomalies are defined as the positive difference between the observed and the background CO mixing ratio. Background CO mixing ratio represents a reference value, not affected by surface emission or pollution events. For this reason, it is computed as the monthly climatological median CO of a remote area away from polluted regions, in the UT_{cruise} (during the whole study period 2002–2020) (Sect. S4 for more details). We performed an evaluation of SOFT-IO for the lower troposphere (LT, surface–750 hPa), the mid troposphere (MT, 750–350 hPa), and upper troposphere (UT, 300–200 hPa). Our simulations detect CO anomalies at the same rates as Sauvage et al. (2017). On average, SOFT-IO underestimates the observed CO anomalies by 10 ppb in the MT and UT, and by 45 ppb in the LT. A sensitivity test has shown absolute differences of 27% in the LT, 16% in the MT and 10% in the UT between SOFT-IO simulations using AN emissions from MACCity and from CEDS2. This clearly highlights the large uncertainty stemming from uncertainties in AN emissions. Another source of uncertainty comes from the definition of background CO. In order to assess this source of uncertainty, we used the 600–300 hPa median CO mixing ratio as background for each site. The differences between the two backgrounds are within 2.5-60 ppbv. Nevertheless, using the alternative background did not make any difference in the anomaly source attribution and in the relative contributions.

2.3 IASI-SOFRID observations

The IASI sensor onboard MetOp-A (launched in 2006) has a 12 km footprint at nadir and a 2200 km swath allowing an overpass twice daily at 9:30 and 21:30 local solar time. IASI provides information for the atmospheric composition e.g. content of trace gases such as O_3 (Eremenko et al., 2008; Barret et al., 2011; Boynard et al., 2016), CO (George et al., 2009; De Wachter et al., 2012) and N_2O (Barret et al., 2021). We use O_3 (v3.5) and CO (v2.1 up to 2014, and v2.2 up to 2019) IASI retrievals performed with SOFRID (Barret et al., 2020; De Wachter et al., 2012).

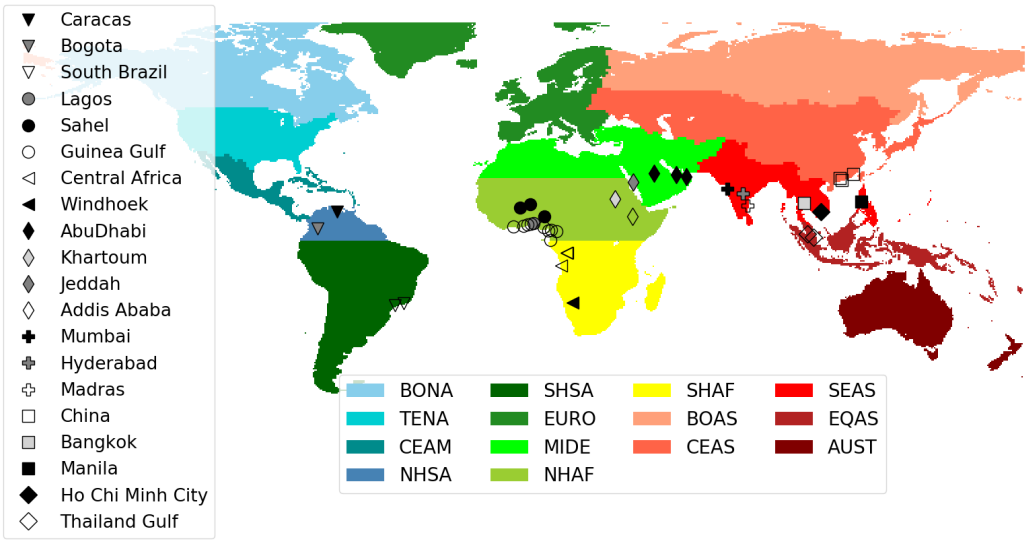

Figure 1. Locations of tropical sites served by IAGOS, and geographical source regions used in SOFT-IO model. BONA: Boreal North America; TENA: Temperate North America; CEAM: Central America; NHSA: Northern Hemisphere South America; SHSA: Southern Hemisphere South America; EURO: Europe; MIDE: Middle East; NHAF: Northern Hemisphere Africa; SHAF: Southern Hemisphere Africa; BOAS: Boreal Asia; CEAS: Central Asia; SEAS: SouthEast Asia; EQAS: Equatorial Asia; AUST: Australia and New Zealand.

SOFRID-O_3 v3.5 retrievals use a dynamical a priori profile based on latitude, season and the tropopause height (Barret et al., 2020). In the tropics, where the surface temperature, thermal contrast and tropopause height are the highest, SOFRID-O_3 retrievals allow two independent pieces of information, one in the troposphere and one in the UTLS (Barret et al., 2020). Comparisons with ozonesonde measurements for the period 2008–2017, showed that SOFRID-O_3 is biased low in the tropical troposphere and UTLS, by 3 $\pm$ 16 % and 12 $\pm$ 33 % respectively in the Northern Tropics (0–30°N), and by 8 $\pm$ 14 % and 21 $\pm$ 30 % in the Southern Tropics (0–30°S) (Barret et al., 2020). The measurements above Northern Africa are erroneous, due to retrieval problems in the presence of desert ground with sand emissivity interfering with the O_3 signature (Boynard et al., 2018). The stripes along the 10°latitude bands in IASI O_3 maps (Fig. 2 e–h and q–t) are due to the use of a dynamical a priori profile, resulting in discontinuities between adjacent latitude bands with different a priori profiles. Nevertheless, the use of a dynamical a priori profile largely improves the retrieved O_3 profiles in terms of biases, variability and correlation relative to the previous version based on a single a priori profile (Barret et al., 2020).

For SOFRID-CO v(2.1 and 2.2 after 2014), two independent pieces of information are provided in the low and upper troposphere (De Wachter et al., 2012). IASI correctly captures the seasonal variability of CO over southern Africa (Windhoek) and European mid-latitudes (Frankfurt) in low (resp. upper) troposphere relative to IAGOS data (resp. correlation coefficients of 0.85 (0.70)). At Windhoek, SOFRID-CO is biased low in the low (resp. upper) troposphere by 13 $\pm$ 20 % (resp. 4 $\pm$ 12 %).

We use monthly averaged SOFRID-CO and O_3 retrievals on a 1° x 1° grid from 2008–2019. We focus on daytime measurements when larger thermal contrast between the surface and the atmosphere results in increased sensitivity of the instrument (Clerbaux et al., 2009) and on pressure levels corresponding approximately to the independent pieces of information: low troposphere defined between 900–700 hPa (LT_{iasi}), mid troposphere between 600–400 hPa (MT_{iasi}) and upper troposphere between 290–220 hPa (UT_{iasi}).

3 Results

3.1 Regional characteristics of tropical O_3 and CO

Figure 2 displays the horizontal distributions of CO in LT_{iasi} (a–d) and UT_{iasi} (i–l and q–t), and of O_3 in the MT_{iasi} (e–h) and UT_{iasi} (m–p and u–x). The results shown in Fig. 2 (a–d) motivated our choice in combining IAGOS sites in clusters when it is necessary to increase the number of measurements. The LT_{iasi} CO maxima, like over the Gulf of Guinea, cover a wide area. Thus, cities located close to each other are likely to experience similar air masses. According to the wind maps they are also affected by similar meteorological conditions (Fig. S3).

Figures 3, 5, 6, 7 (panels 1 and 2) display the monthly average vertical distributions of O_3 and CO based on IAGOS data, for the African, Asian, South American, Arabian and Eastern African clusters. Panels 3 to 5 represent the mean contribution to these CO mixing ratios from AN and BB emissions as estimated by SOFT-IO, with information about their geographical origin (see Sect. 2.2 and Fig. 1). To better understand O_3 and CO anomalies, Fig. 4 displays the CO contributions in three tropospheric layers related to different dynamical regimes: LT corresponding roughly to planetary boundary layer; MT above, and UT corresponding to the beginning of convective detrainment.

3.1.1 Africa

The striking feature of CO and O_3 over the African clusters is the LT maxima during the dry season (January for the Northern Hemisphere and July for the Southern Hemisphere) (Fig. 3 panels 1–2). CO maximises close to the surface, with larger mixing ratios over Lagos (850 ppb) than Sahel (500 ppb) and Gulf of Guinea and Central Africa (400 ppb). The O_3 gradient close to the surface is likely related to surface deposition and titration by highly concentrated nitrogen oxide (NO)(Monks, 2005) which is expected along the high CO concentration. The O_3 maximum and the elevated CO levels (exceeding 300–500 ppb) at 2.5 km over the four clusters, likely indicate chemically processed air masses.

During the Northern Hemisphere dry season (January), the AN contribution dominates over Lagos (58%) and Sahel (57%), while BB slightly dominates over Gulf of Guinea (53 %) (Figs. 3 panel 3a; A1 panels 1a and 2a; 4a; A2a). Contribution from the Northern Hemisphere African fires is also found over Central Africa, where it intensifies and becomes the only important one between 2 and 4 km (Fig. 3 panel 4a). During transport from Northern Hemisphere Africa, the air masses impacted by BB emissions are chemically processed resulting in the formation of an O_3 secondary maximum of 50 ppb coincident with the CO maximum (Fig. 3 panel 1d and 2d) as described in Sauvage et al. (2005). During the Southern Hemisphere dry season (July),

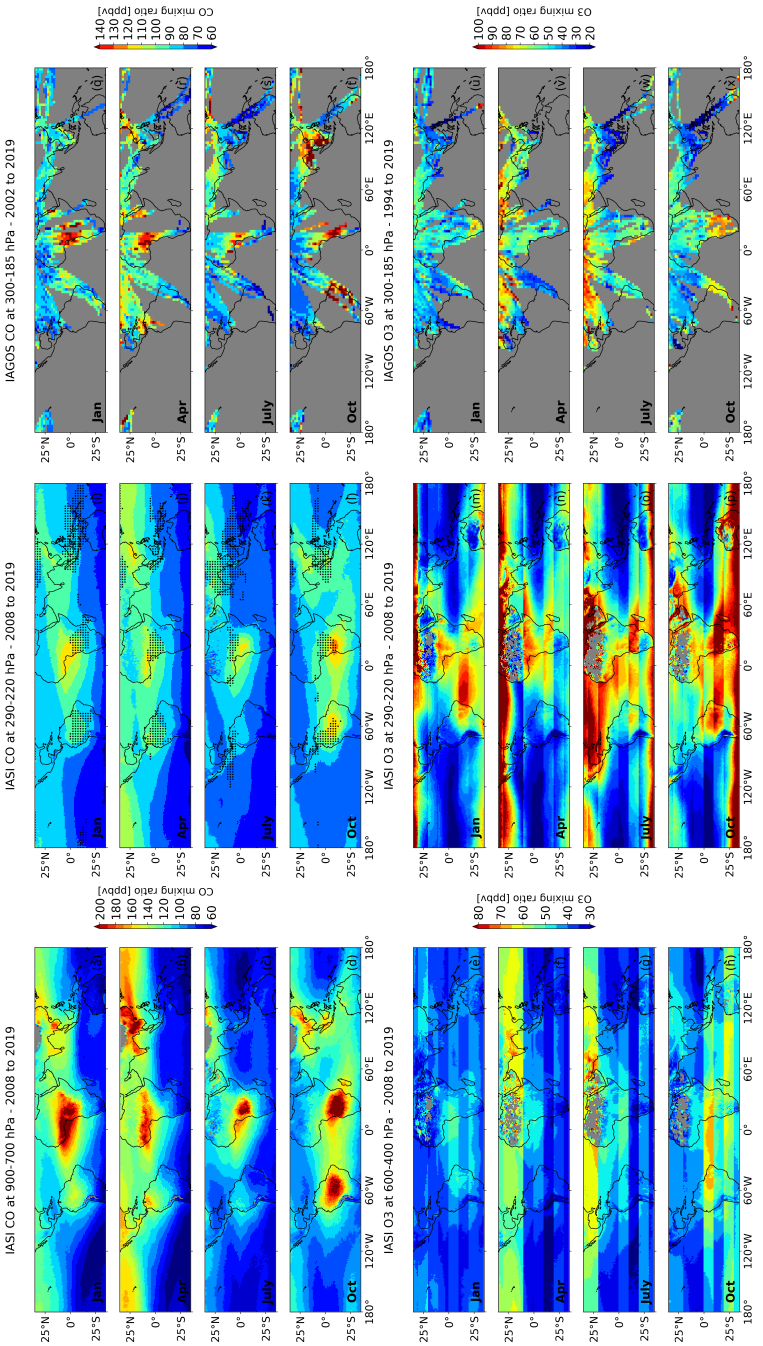

Figure 2. Monthly mean low tropospheric IASI CO distributions (900–700 hPa; a–d), mid tropospheric IASI O_3 distributions (600–400 hPa; e–h), upper tropospheric CO and O_3 distributions based on IASI (290–220 hPa; i–l and m–p resp.) and IAGOS (300–185 hPa; q–t and u–x resp.).

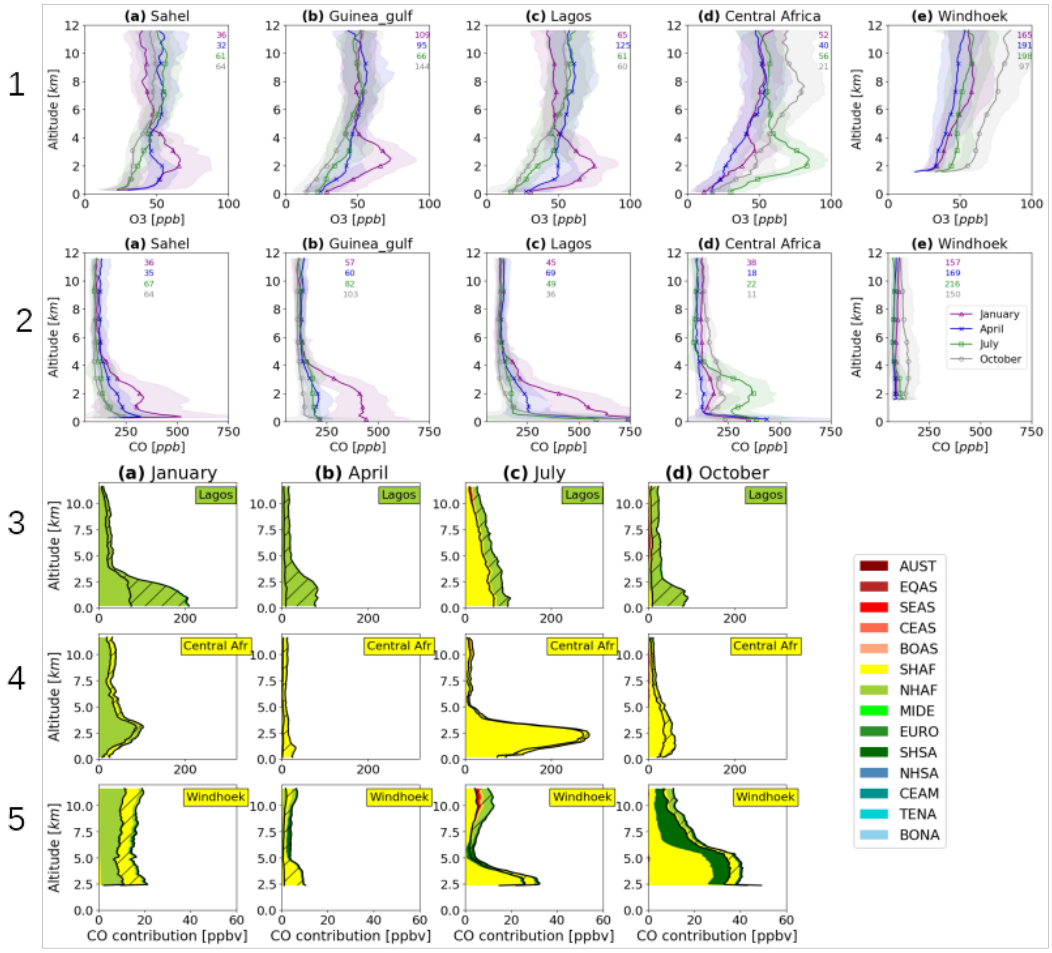

Figure 3. IAGOS monthly mean O_3 (panel 1) and CO (panel 2) vertical distributions. The annotated numbers correspond to the total number of flights per month for the IAGOS period, given in the same colour as in the legend. The shadowed part corresponds to ± 1 one standard deviation. Vertical distribution of CO contributions (in ppb) (panels 3 to 5) with the hatched part showing AN contribution, and the non-hatched part BB contribution. For clarity reasons the CO contribution for Sahel and Gulf of Guinea are displayed in Fig. A1.

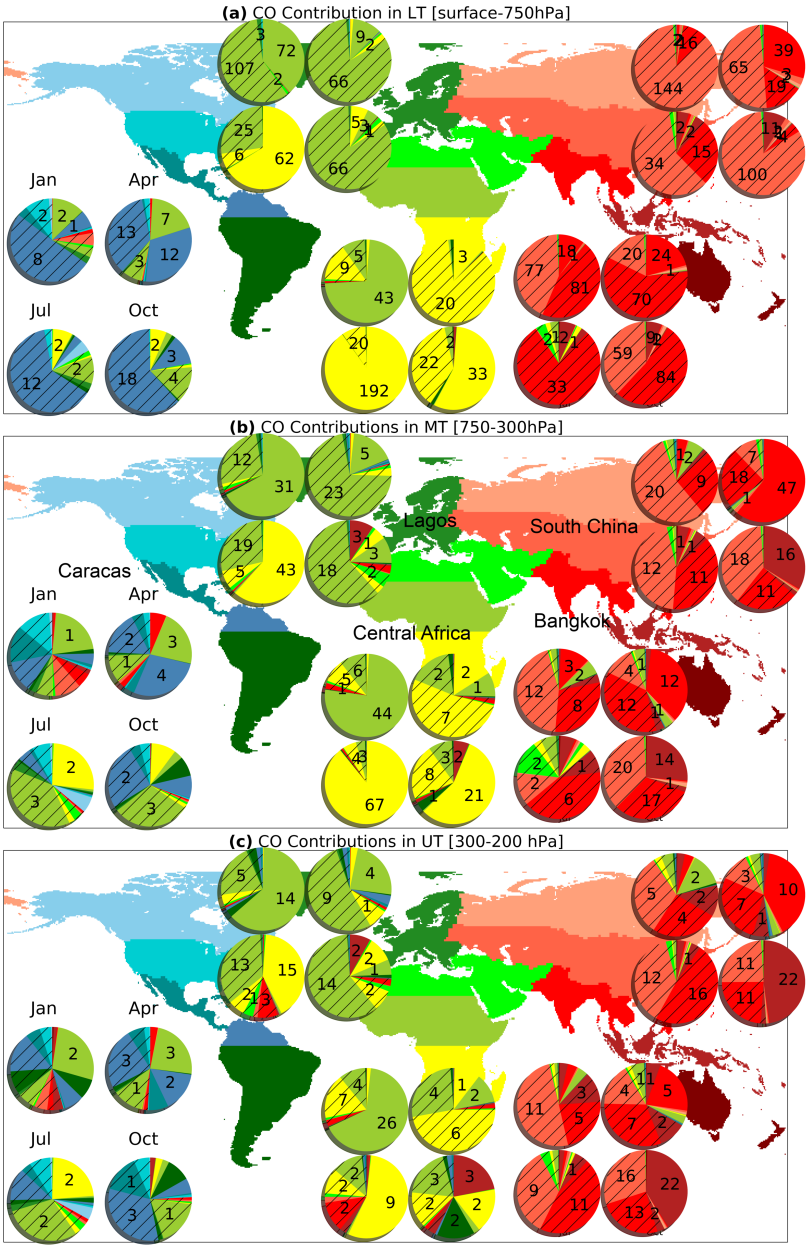

Figure 4. Mean SOFT-IO contributions (in ppb), averaged over all the positive CO anomalies for the tropical sites (Caracas, Lagos, Central Africa, South China and Bangkok) for LT (a), MT (b) and UT (c) for the AN (hatched) and BB (unhatched) contributions. Each pie corresponds to a different month and each group of four pies refer to a different site (see panel b).

the local (Southern Hemisphere Africa) fires are responsible for the CO anomalies over Central Africa in the LT and MT by 90 % (Fig. 4a and b). Impact of these fires is also found in the NT Africa clusters. CO over Lagos is mostly attributed to Southern Hemisphere African emissions (69 ppb) (Fig. 4a), from the surface to about 5 km (Fig. 3 panel 3c). Similar to Lagos, CO over the Gulf of Guinea and Sahel originates from local AN and Southern Hemisphere African BB emissions (Fig. A1 panels 1c and 2c).

The air masses above the fires in NT Africa (resp. ST Africa)(Fig. S1a and S1c resp.) during the respective dry seasons are transported from the continent (Fig. S3a and S3c resp.) by the north-easterly Harmattan flow (resp. the south easterly winds) (Sauvage et al., 2005). This result is clearly consistent with IASI LT_{iasi} CO (Fig. 2a and c) which shows transport from the fire region where the highest concentrations are detected towards Southern Africa in January (resp. the Gulf of Guinea and southern West Africa in July). In the NT, the enhanced O_3 and CO are confined in the low troposphere due to the stability of the Harmattan flow and Saharan anticyclone which prevent vertical mixing (Sauvage et al., 2005).

Over the NT African clusters, secondary CO and O_3 maxima are observed below 4 km (Fig. 3 panels 1a–1c and 2a–2c) during the transition from the Northern Hemisphere dry to wet season (April), when the fires are suppressed (Fig. S1b). LT CO mainly comes from local AN emissions (Figs. 3 panel 3b; A1 panels 1b and 2b). The fact that SOFT-IO attributes approximately 80 ppbv of CO to local AN emissions (Figs. 3 panel 3b; A1 panels 1b and 2b), while the observed anomaly reaches 200–250 ppbv and no or few fires are detected by MODIS (Yamasoe et al. (2015); their Fig.7), indicates underestimation of the Northern Hemisphere African AN emissions. These high CO concentrations in April are detected by IASI in the LT_{iasi} (Fig. 2b) over the whole of West Africa indicating the large-scale extent of the impact of these emissions. The enhanced LT O_3 over the three clusters in April (Figs. 3a–c) indicates possible O_3 formation during the transport of the aforementioned emissions towards Sahel and the Gulf of Guinea. A small O_3 enhancement is also detected by IASI in the MT_{iasi} over West Africa (Fig. 2f). During the dry season, nitrogen is accumulated in soils (Jaeglé et al., 2004). Enhanced NO_x concentrations, possibly due to soil emissions when rains start, also contribute to the O_3 increase over NT Africa in April (Saunois et al., 2009), especially over Sahel (Fig. 3 panel 1a–c) because of higher NO_2 concentrations above dry savannas than over wet savannas and forests (Southern Western Africa) (Adon et al., 2010). After excess nitrogen is consumed, the wet-season NO emissions decrease, contributing less to the local O_3 (Adon et al., 2010).

At Windhoek, O_3 and CO maximise in October after Southern Hemisphere dry season (Fig. 3 panels 1e and 2e). This CO peak has the smallest magnitude among the African clusters (150 ppb at 4 km), while O_3 peak is among the largest, reaching 80 ppb in the UT (11.5 km). The LT CO anomalies over Windhoek in October are mainly caused by local BB emissions (68 % BB versus 12 % AN) (Fig. A2a). These high CO concentrations in October are detected by IASI in the LT_{iasi} (Fig. 2d) over the whole of Southern Africa reflecting the large extent of the impact of these emissions. Using MOPPIT CO and MODIS fire count data, Edwards et al. (2006) also noticed the time lag between the peak of the fires and the CO concentration over Southern Africa. They attributed the lag to smoldering fires at the end of the burning season, characterised by low combustion efficiency and increased CO emissions factors (Zheng et al., 2018b). In addition, there is non-negligible influence from Southern Hemisphere South American emissions (20 % mostly BB)(Figs. 3 panel 5d and A2a). The Southern

Hemisphere South American BB contribution increases with height (30 % contribution in MT and 50 % in UT) contributing to the O_3 maximum observed in the UT (Fig. A2b and c) (Sauvage et al., 2006).

An O_3 enhancement of 80 ppb is also observed over Central Africa at 8 km in October (Fig. 3 panel 1d) highlighting the stronger seasonal variability of MT and UT O_3 in ST than NT Africa related to the intense lightning activity in the Southern Hemisphere and the South Atlantic O_3 maximum (Sauvage et al., 2007b, c). The IASI UT_{iasi} O_3 distribution clearly shows that the O_3 maximum covers the entire region from South America to Africa south of the Equator (Fig. 2l).

The annual minima of CO and O_3 over the African clusters occur during the transition from the wet to the dry season (April for ST and October for NT), when the local fires are suppressed (Fig. S1b and d). Over NT Africa, the O_3 minimum occurs below about 4km (Fig. 3 panel 1a–c). The CO maximum mixing ratio below 1 km is due to local AN emissions (Figs. 3 panel 3d; A1 panels 1d and 2d). In contrast with the other months, the CO mixing ratio above the surface maximum decreases sharply with altitude showing low CO concentrations from 2 km to 12 km. Indeed, in October, the monsoon flow has disappeared and West Africa is impacted by the north easterly trade winds which block the transport of air masses impacted by BB from Southern Hemisphere Africa as is clearly visible on the low tropospheric CO distribution from IASI (Fig. 2d). This is confirmed by the predominant local (Northern Hemisphere Africa) origin of CO over Lagos (Fig. 3 panel 3d).

Interestingly, the annual CO surface maximum in Central Africa Occurs in April, before the beginning of the Southern Hemisphere fires, due to local AN emissions (Fig. 3 panel 4b). The measured CO maxima reaches 350 ppb, while SOFT-IO attributes 40 ppb to the aforementioned sources. This means that Southern Hemisphere African AN emissions are likely underestimated. Above 1km, in the absence of fire contributions, CO remains constant with 100 ppb which is the annual minimum, and the O_3 profile is characterised by a steep gradient and the lowest annual concentrations. IASI LT_{iasi} distribution (Fig. 2b) indicates that the CO minimum measured by IAGOS above 1km over Central Africa in April extends over the whole Central and Southern Africa.

The classical increase of O_3 from the surface to the MT in October and April is due to photochemistry which changes from a net sink to a net source of ozone above 6km, depending on the NO_x concentration (Jacob et al., 1996). In the tropics, photochemical O_3 destruction dominates the low troposphere (Archibald et al., 2020), where water vapour concentrations are high, and in highly polluted regions where there is direct removal by titration with NO (Monks et al., 2015). The vegetation can also act as a rapid sink for O_3 via dry deposition (Cros et al., 2000). The lack of these sinks in the MT and UT, coupled with lower water vapour concentrations leads to an increase of O_3 with altitude (Archibald et al., 2020). Lightning can also increase O_3 mixing ratios in the MT and UT (Barret et al., 2010).

3.1.2 Asia

Over the Asian clusters, the annual CO maximum close to the surface occurs in January (except over Manila and the Gulf of Thailand)(Fig. 5 panel 2), due to the lowest boundary layer height in winter, and is mainly attributed to local AN emissions (Figs. 5 and A1 panels 3a, 4a, 5a). Over the Indian and South China clusters, local AN emissions (SouthEast and Central Asian resp.) are dominant, with contributions from 85 to 95 % (Figs. 5 panels 3a and 4a; A1 panel 3a and 4a, and 4a). AN Central Asian emissions mainly control the LT CO anomalies over the Asian clusters (except Bangkok) in January from 52 % (over

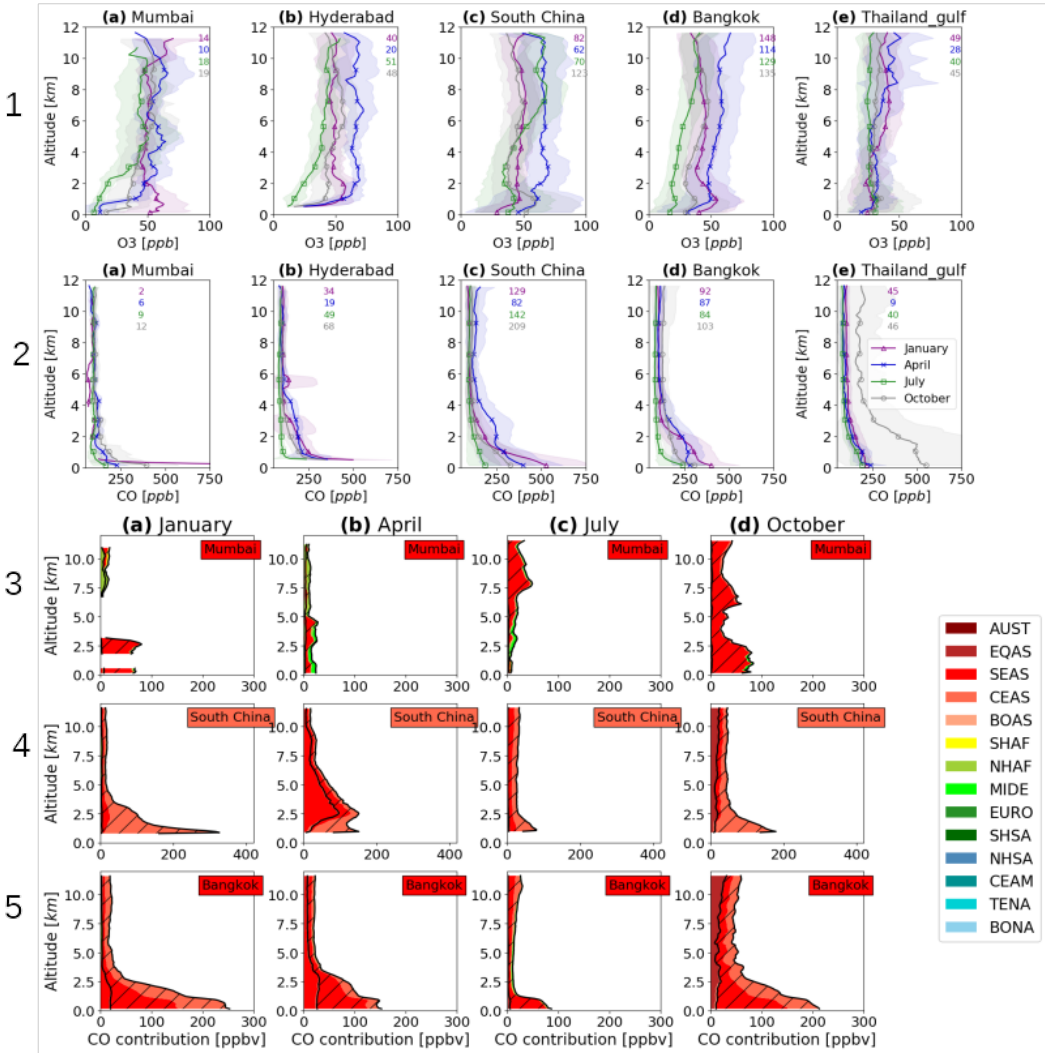

Figure 5. Same as Fig. 3 for the Asian clusters.

Gulf of Thailand) to 75 % (over Manila) (Figs. 4a, A2a and A3a) due to their advection by the northeasterly trade winds. The elevated CO mixing ratios below 2.5 km over the Asian clusters in January are coincident with O_3 enhancements (Figs. 5 panel 1) due to the chemical ageing favoured by: i) the confinement of the CO-rich air masses due to the large-scale subsidence (Lelieveld et al., 2001) and ii) the cloud free conditions. This O_3 enhancement described in Barret et al. (2011) for South Asia during the post monsoon is also detected by IASI (Fig. 2f).

During the pre monsoon season (April), CO and O_3 are both enhanced above the boundary layer and below 4 to 6 km over most sites (Fig. 5 panels 1 and 2). Local AN emissions control the CO anomalies over the majority of the sites (Figs. 5 panels 3b–5b; A1 panels 3b–7b), while spring SouthEast Asian fires impact South China, Bangkok, Ho Chi Minh City and Manila

by 20–30 % in the LT and MT (Figs. 4a and b; A3a and b). In spring the fires are mostly above East Asia and especially the region of Myanmar, Northern Thailand and Laos (Fig. S1b) and the corresponding large CO concentrations are captured by IASI (Fig. 2b). The BB outflow towards South China and the Pacific ocean is due to westward low and mid tropospheric winds (Figs. 2b and S3b and S3f). The enhanced MT O_3 is attributable to the intense solar radiation associated with the important amounts of precursors from AN and BB emissions which were previously evidenced. This is in agreement with the observed O_3 maximum in spring over South China (Dufour et al., 2010) and Bangkok (Sahu et al., 2013). Yarragunta et al. (2019) found that local AN emissions are responsible for the CO and O_3 abundances over South India during the pre-monsoon season. This is in accordance with the SOFT-IO contributions over the Indian clusters (Figs. 5 panels 3b; A1 panels 3b and 4b; A3a). CO anomalies over Mumbai are also caused by transport of AN emissions from the Middle East (36%) in the LT, and Northern Hemisphere Africa (30%) in the MT (Fig. A3a and b). In the UT, the impact of Northern Hemisphere African (AN and BB) emissions dominates over Mumbai (54 %) and Hyderabad (50 %). It has to be noted that the number of profiles over Mumbai (6) and Hyderabad (19) are lower than the threshold established for representativeness (see Sect. 2.1.1). The UT_{iasi} CO and O_3 transport from Northern Hemisphere Africa towards the Arabian sea and South India is also captured by IASI (Figs. 2j and 2n), indicating O_3 photochemical production during the transport.

The BB contribution is also important during the post monsoon season (October) because of active fires over Indonesia (Fig. S1). The Gulf of Thailand cluster is the most affected, from the surface (600 ppb) to the UT (Fig. 5 panel 1e). IASI CO data (Fig. 2d) and wind fields (Fig. S3d) show that the LT_{iasi} CO-rich air masses impacted by the fires (Fig. S1d) are advected towards the South East Asian coastal clusters (South China, Gulf of Thailand, Bangkok and Manila), as confirmed by the SOFT-IO (contributions of 10 % on average) (Figs. 5 panels 4d and 5d; A1 panels 6d and 7d; 4a; A2a and A3a). The collocated O_3 enhancement (below 2 km) over these clusters (Figs. 5 pane 1c–1e) indicates O_3 production by BB and AN precursors. The Equatorial Asian BB contribution intensifies in the UT, over the SE Asian coastal clusters (40–57 %), Madras (50 %) and Hyderabad (33 %) (Figs. 4c; A2c and A3c). The upper tropospheric CO maximum above the fires is also captured by IASI and IAGOS (Figs. 2l; 2p and S1d). Based on MLS CO data, Livesey et al. (2013) also found an upper tropospheric CO maximum over Indonesia and attributed it to episodically strong convection, in agreement with the low OLR in Fig. 2p. In contrast, the UT_{iasi} and MT_{iasi} O_3 distribution show a SE-NW gradient (Figs. 2l and 2h) with lower O_3-levels over the Maritime continent and the southern Indian Ocean and higher ones over India and the Arabian sea. This was reported by Barret et al. (2011) as a result of convection over the first region and subsidence of precursor enriched air masses over the second one.

The LT O_3 and CO mixing ratios over the Asian clusters minimise during the summer monsoon (July) (Fig. 5 panels 1–2). The reversal of the north-easterly trades to the monsoon flow (Fig. S3c) results in advection of O_3- and CO-poor air masses from the Indian ocean towards Asia. Furthermore, cloudy conditions scavenging of O_3 precursors result in lower O_3 production than in clear sky conditions (Mari et al., 2000; Safieddine et al., 2016). The steep CO gradient close to the surface (below 1 km) indicates the convective uplift of polluted boundary layer air masses towards the UT. The resulting enhancement of CO in the UT within the Asian monsoon anticyclone (AMA) analysed in Park et al. (2008) and Barret et al. (2016) is clear from IASI (Fig. 2k). In contrast, the positive South-North O_3 gradient between the Maritime continent and north South Asia and Middle

East (Figs. 2o and w) is associated with: i) the photochemical ageing of air masses while they are recirculating towards Middle East (Lawrence and Lelieveld, 2010) and ii) the high insolation over Middle East (Barret et al., 2016).

3.1.3 South America

One common characteristic among the South American clusters is the increase in O_3 from the surface to the MT (Fig. 6 panel 1). This is due to the lack of depositional and chemical sinks above the low troposphere, in combination with lower water vapour concentrations, and lightning emissions, as discussed in Sec. 3.1.1. In Caracas, O_3 shows one maximum in the LT and one in the MT in April. Over Bogota and SBrazil O_3 peaks in October over the whole troposphere with mixing ratios reaching 45 and 60 ppb in the UT. For Bogota (resp. SBrazil) the tropospheric O_3 annual minimum occurs in July (resp. April). As IAGOS over SBrazil below 6 km, the IASI distributions over tropical South America (Fig. 2 e–h) display MT_{iasi} O_3 in January and April than in July and October.

Another common characteristic among the three clusters is the LT CO maximum in April (Fig. 6 panel 2). The CO mixing ratios peak over Bogota below 1km (400 ppb) and over Caracas up to 2km (200 ppb). According to SOFT-IO, the CO maximum over Caracas is due to local AN (35 %) and BB (32 %) emissions (Northern Hemisphere South America) (Figs. A2, and 6 panel 5b). Similar contributions are found over Bogota (Fig. 6 panel 4). This local origin of emissions is corroborated by the elevated IASI LT_{iasi} CO mixing ratios (Fig. 2b) collocated with the strong AN emissions above Colombia and Venezuela, and active fires above the latter (Figs. S1b and S2b). Transport also plays an important role with 20 % of the anomalies caused by BB Northern Hemisphere African emissions (Fig. 4a). The O_3 maximum collocated with the CO one at 2 km over Caracas (Fig. 6 panels 1a and 2a), indicates O_3 production during transport of Northern Hemisphere African air masses impacted by BB. The second O_3 maximum above 5 km over Caracas is also noticed by Yamasoe et al. (2015) that attributed it to local AN sources followed by lightning.

Over SBrazil, the annual CO maximum below 1.5 km in April (Fig. 6 panel 2c) is due to local AN emissions (Fig. 6 panel 5b) located over the southern part of Brazil (Fig. S2b). The observed CO enhancement reaches 350 ppb, while SOFT-IO attributes 65 ppb to the aforementioned emissions. This indicates that Southern Hemisphere South American AN emissions are underestimated by SOFT-IO. The observed CO enhancement at 1.5 km is new compared to Yamasoe et al. (2015) and is related to increased local AN contributions for March–April–May 2014 relative to the previous years. This is in agreement with the CEDS inventory, which shows a peak in AN emissions over South Brazil (18–29° S and 35–52° W) in 2014, mostly coming from the transportation sector (Fig. not shown).

The CO minima over the three clusters are observed in January, when CO concentrations are below 300 ppb (resp. 180 ppb) over Bogota (resp. Caracas and SBrazil) below 1km (Fig. 6 panel 2). The CO mixing ratios decrease below 100 ppb above the polluted layers all year long, with exception of SBrazil, where a first maximum (150–200 ppb) occurs between 2–4 km and a second one (200–250 ppb) above 8 km in October. IASI clearly detects the MT_{iasi} and UT_{iasi} (Fig. 2d and p resp.) maxima over most of tropical south America in October.

From SOFT-IO we can see that, over SBrazil in October, CO enhancement below 1 km is caused by local AN (52 %) and BB (44 %) emissions (Fig. 6 panel 5d). In the MT and UT, the BB contribution exceeds 80 % because of the strong convection

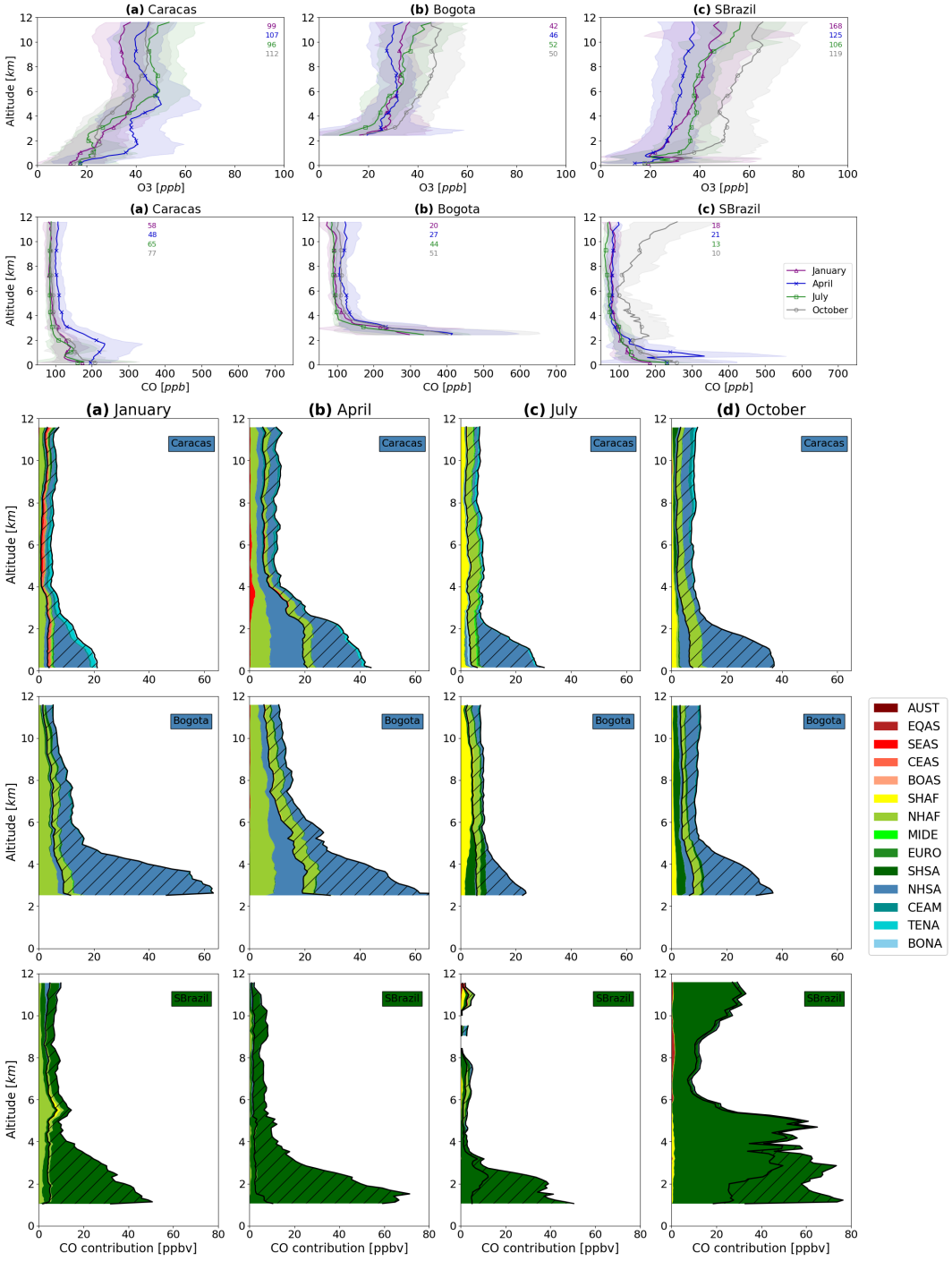

Figure 6. Same as Fig. 3 for the South American clusters.

moving over the BB regions (Liu et al., 2010), documented by low OLR (Fig. 2l). The uplifted BB products are trapped in an anticyclonic circulation developed over Central South America (Fig. S3l). CO from Southern Hemisphere South American fires are transported over Bogota, at the edge of the anticyclone, but does not reach Caracas which lies outside of the anticyclone (Fig. 6 panels 3d and 4d). Their photochemical processing contributes to the seasonal O_3 enhancement over South America which is the western part of the wave-one pattern (Thompson et al., 2003b; Sauvage et al., 2006). This is highlighted by the collocation of IASI UT_{iasi} CO (Fig. 2l) and O_3 (Fig. 2p) maxima within the anticyclone.

3.1.4 Arabia and Eastern Africa (AEA)

The striking feature of the AEA clusters is the elevated O_3 centered at around 8 km (70 ppb on average) for all the clusters during April and for the northern clusters of Jeddah and Abu Dhabi during July (Fig. 7 panel 1 a–d). The particularly low CO mixing ratio accompanying the O_3 enhancements (Fig. 7 panel 2a–d) points to a dynamical origin of O_3. Note that only limited number of profiles are available over Abu Dhabi above 10 km and Khartoum in April. The O_3 enhancements over the 4 sites of AEA and the anticorellation with CO, are also detected by IASI in the MT_{iasi} and UT_{iasi} (Fig. 2j, k, n and o).

Tropopause foldings in the vicinity of the subtropical jet stream are associated with downward transport of stratospheric ozone (Stohl et al., 2003; Lelieveld et al., 2009; Safieddine et al., 2014) resulting in a tropospheric O_3 enhancement during spring and summer (Tang et al., 2011). This is in agreement with Cohen et al. (2018) that found the maximum O_3 to CO ratio over the Arabian peninsula for the same seasons (their Fig. A1), using IAGOS data for the period 1994 to 2013. Also, large O_3 regional enhancements are detected by IASI over the Arabian sea similarly to Jia et al. (2017) based on TOC from OMI/MLS. Jia et al. (2017) attributed these O_3 enhancements to emissions from India (50 %), with smaller contributions from the Middle East and Africa (30 %). This is in agreement with SOFT-IO, which shows a significant contribution from SouthEast Asia over Jeddah (29 %) and a lower one over Addis Ababa (7%) (Figs. 7 panels 4b and 5b, and A2a). SOFT-IO also attributes large contributions from Northern Hemisphere African AN and BB emissions over Abu Dhabi and to a lesser extent over Khartoum (Fig. 7 panels 3b and 6b). The contribution of American sources over Abu Dhabi indicates eastward transport, which is not present in the rest of the AEA clusters because Abu Dhabi is affected by the subtropical westerly jet in the UT. In contrast the rest of the AEA clusters are affected by the tropical easterly jet which brings CO from Asian regions.

In July, the Middle East summer O_3 maximum is also partly related to subsidence of AMA air masses which brings O_3 produced from South Asian AN and $LiNO_x$ emissions (Barret et al., 2016). The polluted air masses from South and SouthEast Asia uplifted by monsoon deep convection are trapped in the AMA which extends westward to Northeast Africa and the Middle East (Barret et al., 2016; Park et al., 2007). Over Khartoum and Jeddah (resp. Addis Ababa and AbuDhabi) 20 ppb (resp. 10 ppb) of CO originates from SouthEast Asia at 6–12 km. The impact of the SouthEast Asian emissions is stronger over Jeddah (78 %) than over Khartoum (60 %) and Addis Ababa (46 %) (Fig. A2c) which are outside of the AMA (Fig. 7 panel 1). Furthermore, the O_3 minimum over Addis Ababa (45–50 ppb) is related to the ITCZ located between 5° N and 10° N during the Northern Hemisphere wet season (Lannuque et al., 2021). The UT_{iasi} O_3 enhancement over Arabia and the Arabian sea, and the transition to lower concentrations south of the tip of Arabia are also clear with IASI (Fig. 2c). The O_3 minimum over Africa is caused by uplift of local African O_3-poor air masses from the surface to the ITCZ (Lannuque et al., 2021). The

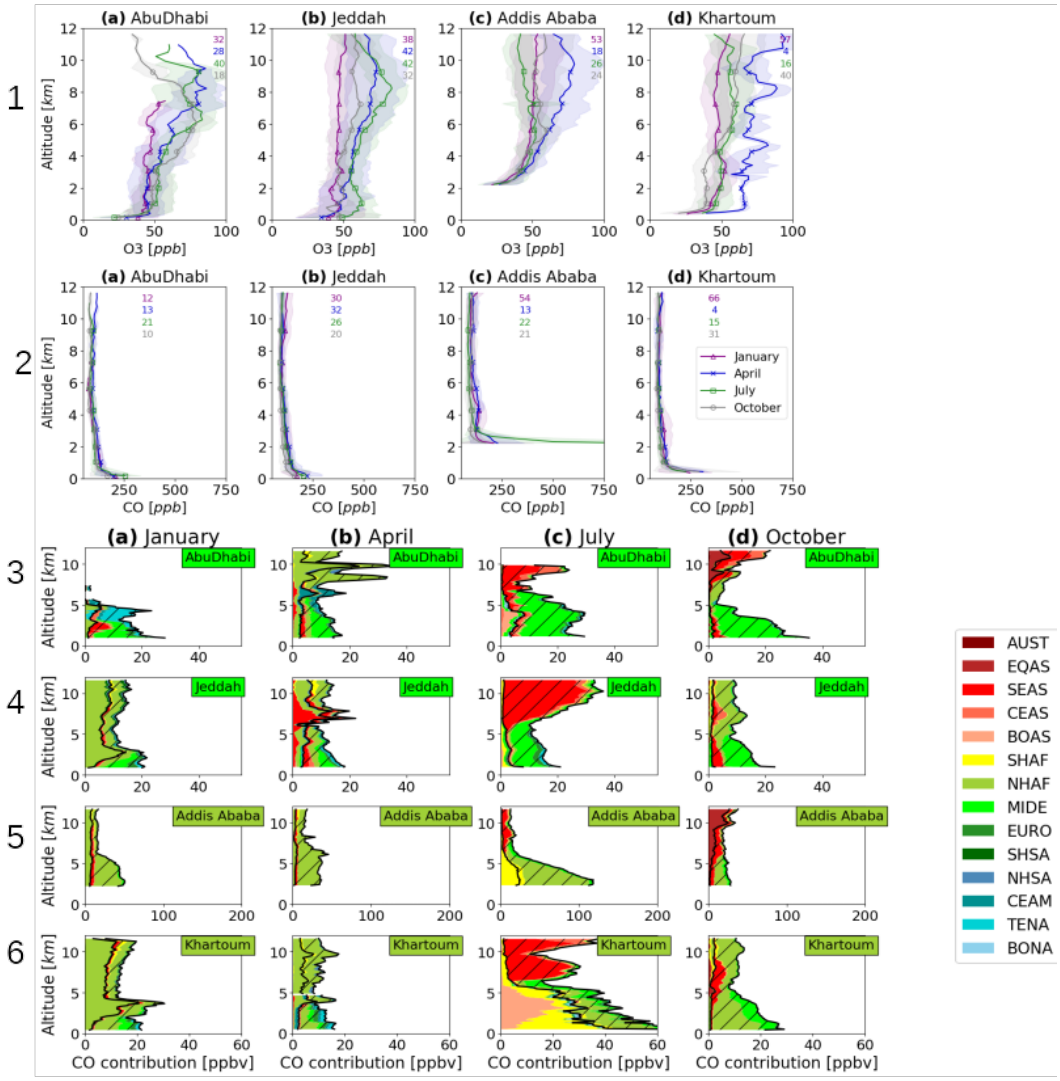

Figure 7. Same as Fig. 3 for the Arabian and Eastern African clusters.

increase of O_3 northwards (such as over Khartoum with 60 ppb; Fig. 7 panel 1d) is due to the O_3 production within uplifted CO-rich air masses, transported away from the ITCZ by the upper branches of the Hadley cell (Lannuque et al., 2021).

One common characteristic among the AEA clusters is the elevated CO mixing ratio in the surface layer (below 1km) all year long (Fig. 7 panel 2). The surface maximum is larger over Addis Ababa (700 ppb in July) and Khartoum (350 ppb in April), than in Jeddah and AbuDhabi (<250 ppb). Over the East African sites (Khartoum and Addis Ababa), a layer of enhanced CO is observed below 4 km, in January and April. This winter to spring high CO layer in the LT_{iasi} over Eastern Africa is detected by IASI which clearly shows that it does not reach Arabia (Fig. 2a–b).

In January, the surface CO maximum is mostly controlled by local AN emissions over the AEA clusters (Figs. 7 panels 3a to 6a). Strong AN emissions from Northern Hemisphere Africa control the CO anomalies over Addis Ababa with contribution of 71 % in the LT and 58 % in the MT (Fig. A2a). Influence from the Northern Hemisphere African fires is also evident (12 % in the LT and 20 % in the MT) (Fig. A2a). The impact from these fires intensifies over Khartoum and Jeddah between 2 and 4 km with contributions of 58 % and 53 % respectively (Fig. A2a). The effect of the Northern Hemisphere African emissions towards Eastern Africa and Jeddah is also detected by IASI (Fig. 2a), which shows a negative eastward CO gradient. The co-occurring O_3 enhancement (Fig. 2e) over Khartoum and Jeddah below 4 km reflects O_3 formation during transport from the fires (Fig. 7 panels 1b and 1d).

In July, the CO surface maximum is again caused by local AN emissions (Fig. 7 panels 3c–5c), except over Khartoum where air masses from Southern Hemisphere African fires are the dominant source of CO (Fig. 7 panel 6c). The combination of local AN (70 %) and Southern Hemisphere African BB (23 %) emissions is responsible for the annual CO maximum at the surface over Addis Ababa (Figs. 7 panel 5c, and A2a). Interestingly, the impact of the Southern Hemisphere African fires below 4km over Khartoum and Addis Ababa is stronger than the impact of local fires during the respective dry season (Figs. 7 panels 5ac and 6ac). The O_3 enhancement below 4 km over the Jeddah, Khartoum and Addis Ababa indicates O_3 production during the transport of CO-rich air masses impacted by the Southern Hemisphere African fires (Fig. 7 panels 1 j to l). In contrast, over Abu Dhabi the O_3 enhancements at around 7 and 10 km (Fig. 7 panel 1a) are likely related to transport of CO-rich air masses from Boreal Asia (Fig. 7 panel 3c).

In October, in the LT the long range transport from Asia (SouthEast AN and Equatorial BB) plays a significant role in CO anomalies over the AEA sites (Figs. 7 panels 3d–6d), especially over Addis Ababa and Jeddah. In the LT_{iasi}, the northeasterlies (Fig. S3d) transport CO-rich air masses from Asia towards eastern Africa as detected by IASI (Fig. 2d).

Above 4km in October, O_3 enhancements are observed over the AEA sites especially over Abu Dhabi which is the eastern-most site of the AEA region (Fig. 7 panel 1). IASI detects a MT_{iasi} O_3 increase above the Arabian sea and Northern India (Fig. 2h). The O_3 enhancement in the MT over the Arabian sea detected with ozone soundings during the INDOEX campaign (1999–2000) has been attributed to Indian sources uplifted over the marine boundary layer by the sea breeze circulation in Lawrence and Lelieveld (2010) and was further analysed and documented with IASI data by Barret et al. (2011). The O_3-rich air masses are further transported towards Eastern Africa by the prevailing northeasterlies (Fig. S3h) as documented by the predominant SouthEast Asian origin of MT and UT CO over the AEA sites (Figs. 7 panels 3d and 6d).

Table 2. Total (AN + BB) CO emission rates (in $10^{-10}\,kg\,m^{-2}\,s^{-1}$) based on CEDS and GFAS emission inventories over West Africa (10° W–12.5° E; 0–12.5° N), Central Africa (10–35° W; 2.5–20° S), East Asia (92.5–110° E; 10–27° N), Maritime Continent (93–121° E; 10° S–10° N), South Brazil (35–50° W; 0–20° S) and Arabia and Eastern Africa (30–60° E; 5–25° N).

	West Africa	Central Africa	East Asia	India	Maritime Continent	South Brazil	AEA
January	6	1	4	3	1.5	1	1.5
April	3	1	11	3.5	1.5	0.5	1
July	2.5	10	3	3	2	1	0.5
October	2.5	3	3	3	6	4	1
Annual	3.5	3.7	5.5	3.1	3	1.5	1

3.2 Control factors of tropical O_3 and CO

Figure 8 displays the annual maximum/minimum of O_3 (a) and CO (b) mixing ratios and their corresponding mean height. The annual maxima/minima are calculated based on monthly averaged mixing ratios over vertical layers with 40 hPa thickness. Figure 9 displays the transport pathways of CO emissions from the African, South American and Asian source regions, towards the 20 tropical sites in the LT (a), MT (b) and UT (c). We show the source regions and the months corresponding to the largest amounts of transported CO (in ppb). Figure 10 displays the AN and BB contribution to CO anomalies (in ppb) over the tropical UT_{cruise}.

Overall, the CO profiles above all tropical clusters display an annual maximum above the surface layer (approximately at 0.5 km) (Fig. 8b). This is also valid for Caracas, Bogota, Windhoek and Addis Ababa which are located at high altitude above the sea surface (with a mean elevation of 0.9 km, 2.6 km, 1.6 km and 2.3 km respectively). For all the clusters located in the NT (except the Gulf of Guinea and Caracas), the CO-polluted boundary layer, is mainly attributed to local AN emissions, even for Lagos and Sahel, where BB is expected to be of great importance (Reeves et al., 2010; Mari et al., 2008). This finding confirms the key role of AN emissions in the Northern Hemisphere, related to larger population compared to the Southern Hemisphere, and enhanced AN urban and industrial activity. Concerning the ST, the surface-layer pollution is predominantly caused by BB over ST Africa (Central Africa and Windhoek) during the dry season (Figs. 4, A2), and by AN over the SBrazil (Fig. A2). The CO maxima over the latter occurs before the burning season. This is in accordance with previous studies suggesting fossil fuels as the main CO source over Sao Paulo and Rio de Janeiro (Alonso et al., 2010), and decreasing BB over South America (Andela et al., 2017; Deeter et al., 2018) due to the long-term declining deforestation rates, especially over forested areas ($\approx$ 54 %) and over savanna and shrublands ($\approx$ 39 %) (Naus et al., 2022). The importance of the AN emissions is also evident over Central Africa, where a polluted surface layer is present all year long and during the transition seasons, when the fires are suppressed, it is largely caused by AN contributions (40 % and 86 % in April and October; Fig. 4a). Thus, the impact of the AN emissions is also important in the ST.

The CO maxima show strong variations in terms of magnitude and season among the tropical clusters because they are mostly caused by local emissions with varying intensity and seasonal pattern, depending on the region. In contrast, the CO

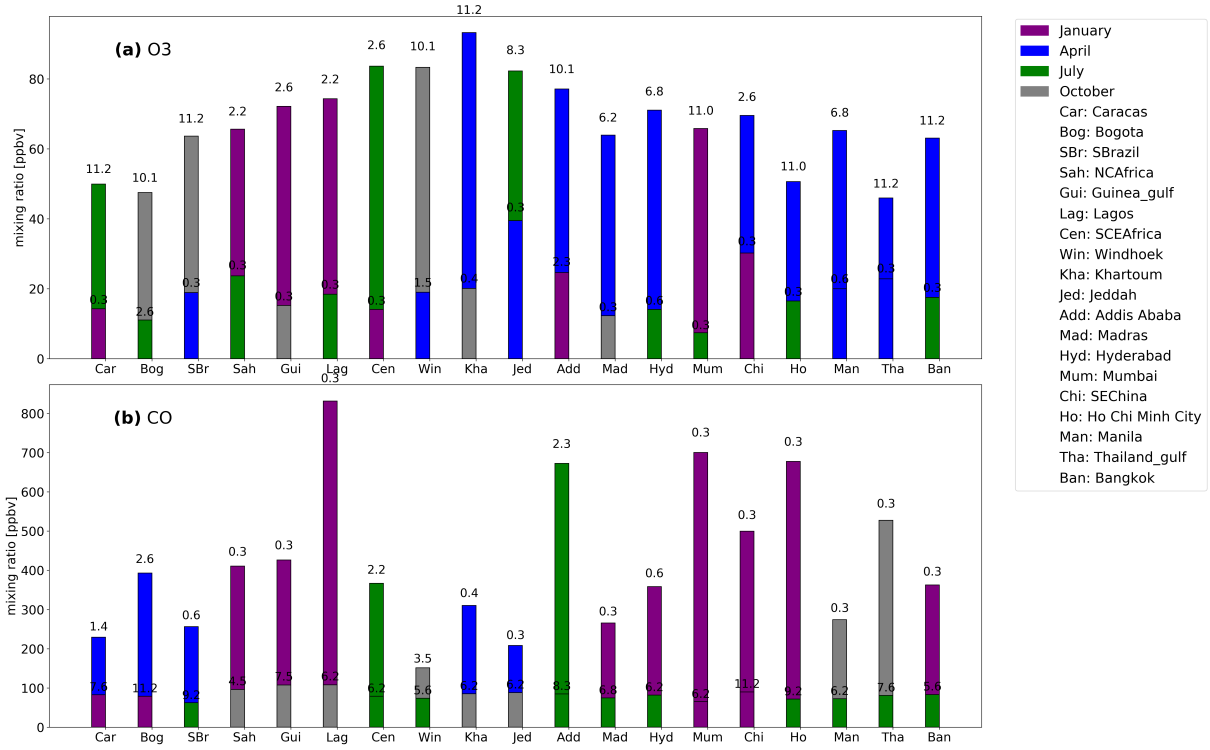

Figure 8. O_3 (a) and CO (b) annual maximum (higher bar) and minimum (lower bar) mixing ratio observed over the tropical clusters. The annotated number on top of each bar indicates the altitude (in km) of the observed annual maximum/minimum mixing ratio. The colour in the bar indicates the month of the maximum/minimum.

minima are uniform in terms of intensity levels of mixing ratios, close to the CO background levels, due to mixing and transport over the lifetime of CO. As expected, they occur in the MT or UT, in the absence of the emissions and where CO is chemically destroyed. As for the CO maxima, their strong seasonality is related to the seasonality of the surface emissions and the meteorological conditions, which differ over each region. Further discussions on the magnitude and the seasonality of the CO maxima and minima will follow later.

Because of its complex chemistry, the situation for O_3 is more complicated. Africa is the only region where the annual O_3 maximum occurs in the LT (at 2.5 km) during the dry season (Fig. 8a Sahel, Guinea Gulf, Lagos and Central Africa). The co-occurrence of maximum O_3 with the maximum in CO over Africa during the local fires indicates stronger dependency of O_3 on the surface AN and BB CO emissions for these regions, in agreement with Sauvage et al. (2007b). South China is the only Asian cluster where the annual O_3 maximum is observed in the LT (at 2.6 km) during the active local fires (April). In contrast, over the other regions, the annual O_3 maximum is observed above 6 km (Fig. 8a). This indicates that O_3 is likely associated with larger ozone production efficiency in the MT and UT (Sauvage et al., 2007c). In regions such as Arabia (Jeddah and Abu Dhabi), the lack of CO enhancement in the UT indicates dynamical origin of O_3 (e.g. stratospheric influence and transport of

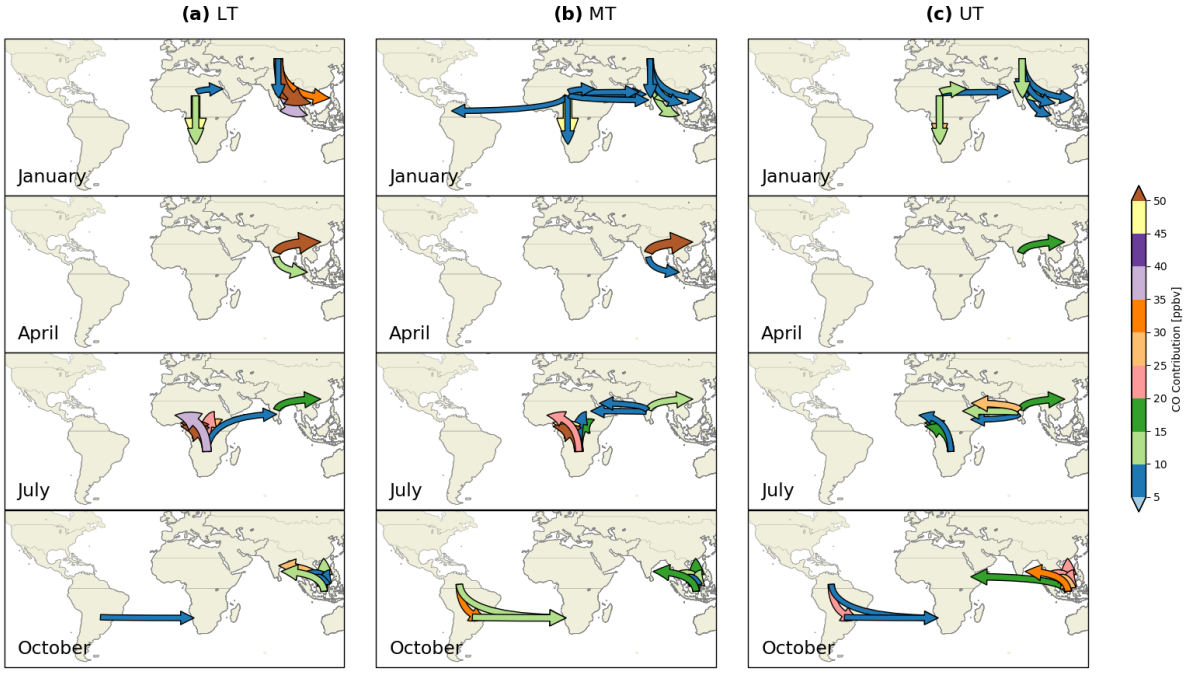

Figure 9. Transport of CO (AN+BB) emissions from the African, South American and Asian source regions towards the 20 tropical sites taken into account for this study. The colorbar shows the amount of CO transported in ppb.

O_3 and precursors from Asia; see Sec. 3.1.4). In contrast, in regions such SBrazil and Windhoek in October, the co-occurrence of O_3 and CO enhancement in the MT and UT indicates O_3 production from surface sources (e.g. fires). In addition, LiNOx emissions can contribute to O_3 production at higher altitudes (Secs. 3.1.1 and 3.1.3). The annual O_3 minima for all the tropical clusters are observed close to the surface (below 0.5 km on average) (Fig. 8a). This is likely related to deposition and titration by NO (see Sect. 3.1.1 for more details).

The highest CO and O_3 maxima among all the tropical clusters occur over NT Africa in the LT (at 0.3 km for CO and 2.5 km for O_3) during the dry season (January) mostly due to local AN emissions (over Lagos and Sahel) and BB (over Guinea Gulf). Table 2 displays the total (AN and BB) CO emissions rates over several regions of interests based on the sum of CEDS and GFAS emission inventories. The NO_x-limited O_3 production regime over Western Africa (Saunois et al., 2009; Zhang et al., 2016) likely explains the O_3 maxima when the local emissions, and thus the NO_2 concentration (Jaeglé et al., 2004), intensify in the region. The largest O_3 and CO mixing ratio over Lagos (Fig. 8) is due to its proximity to the strong Nigerian AN emissions, as confirmed by SOFT-IO (see Sect. 3.1.1). The O_3 maxima show smaller variations (of approximately 10 ppb) among the NT African clusters. In contrast to CO, the O_3 enhancement does not strongly depend on the proximity to emissions, as it is produced during the transport and chemical ageing of air masses rich in precursors (Sauvage et al., 2007b).

The second highest CO and O_3 maxima over the tropical regions are observed over Asia (Fig. 8) mostly due to AN emissions. According to Table 2, the CO emissions over East Asia and India are lower than the ones over Western Africa in January. This explains the lower CO mixing ratio over Asia than over Lagos. SOFT-IO seems to represent better the Asian contributions than the African ones. As mentioned in Sect. 3.1.1, the AN emissions over NH and SH Africa are likely underestimated by the SOFT-IO computations (Fig. 3 panels 3b and 4b). This is confirmed by that fact that CO mixing ratio is higher over Africa than over Asia, in contrast to the CO contributions estimated by SOFT-IO.

Previous studies have already found concentrations of pollutants in West Africa (e.g. Lagos, Abidjan, Cotonou) comparable to those observed over Asian megacities (Assamoi and Liousse, 2010; Adon et al., 2016; Sauvage et al., 2007b). The rapid growth over African megacities is responsible for increasing emissions from diffuse and inefficient combustion sources (Marais and Wiedinmyer, 2016), such as residential sources mainly for cooking and heating (Zheng et al., 2019), and traffic emissions (related to large number of two-stroke vehicles, poor fuel quality and poorly-maintained engines) (Assamoi and Liousse, 2010). In contrast, Eastern China has had one of the largest decreases in CO emissions (Hedelius et al., 2021) due to technological changes with improved combustion efficiency (Zheng et al., 2018a), such as replacing residential coal use with electricity and natural gas (Buchholz et al., 2021), and implementation of Clean Air Policies (van der A et al., 2017) around 2010. In India, on the other hand, there are no regulation in the emissions, and this explains the highest CO mixing ratios among the Asian clusters (Fig. 8). Previous studies have already reported increasing CO emissions over India from 1996–2015, due to several factors such as increases in residential and agricultural sources (Pandey et al., 2014) and to power production and transport activities (Sadavarte and Venkataraman, 2014).

As in NT Africa, the CO-rich air masses accumulated in the LT over the Asian clusters in January are accompanied by a secondary LT O_3 maximum. However, these maxima are significantly lower (40–60 ppb) (Sect. 3.1.2) than the NT African ones (65–75 ppb) (Fig. 8a; Sect. 3.1.1), even for clusters with similar LT CO mixing ratios (e.g. Sahel and South China) (Fig. 8a). This is because: i) the CO emissions are less strong over the Asian clusters, as mentioned before, and ii) the O_3 enhancement over Asia is caused by AN-polluted air, while in NT Africa by mixed (AN and BB) polluted air. During the Atom campaign, Bourgeois et al. (2021) found that O_3 levels are more enhanced in mixed air pollution, because they are associated with greater NO_x and peroxy acyl nitrates (a NO_x reservoir compound), and thus increased O_3 production, in comparison to BB- or AN-polluted air alone. This is in agreement with the O_3 annual maximum in April over East Asia (Fig. 8a), over clusters such as South China and Bangkok, which are affected by the local fires.

The highest emission rates over East Asia and India are observed in April (Table 2). In the absence of the stability of the north easterlies, the air masses are not confined close to the surface like in January. Over East Asia, the contribution of the local fires is present in addition to the local AN emissions. The impact of the fires dominates in the MT in clusters such as South China and Bangkok, and is evident over Manila and Ho Chi Minh City (see Sect. 3.1.2). Interestingly, the Northern Hemisphere African fires in January correspond to 72 % of the global burned area, whereas the Northern Hemisphere Asian fires only to the 2.5 % (Van der Werf et al., 2010). However, both regions contribute significantly to the global CO concentrations (44 % for Africa and 22 % for Asia) because of more complete oxidation, and thus reduced CO production, over grass fires (Africa savannas), relative to fires in forests and peatlands (deforestation and peatland fires over Asia) (Van der Werf et al., 2010). The

large extend of the impact of the Northern Hemisphere Asian fires is displayed in IASI, with an outflow towards SE Asian coast and the Pacific (Fig. 2f). The stronger winds in April than in January and the eastwards transport pathway (Fig. 9 panel 1 a–b) leads to lower CO mixing ratio in April, despite the higher emission rates (Table 2).

Concerning India, local AN emissions are responsible for the CO enhancement in April, with negligible BB contribution (Figs. 5 panel 3a and A1 panels 3a and 4a). According to IAGOS and IASI (Figs. 2a–d, 5 panel 1ab), the LT CO over India shows strong seasonal variability which cannot be explained by the weak variations of the Indian emissions (Table 2). This indicates that LT CO over India is rather linked with seasonal changes in the meteorological circulation. Similarly to East Asia, during January the air masses are transported southward due to the north easterlies, while the reversal of the winds to south-westerlies in July results in northward transport (Figs. 2 and S3) (Lawrence and Lelieveld, 2010). Because of this circulation pattern in July, the oceanic influence brings clean air masses over the Asian clusters resulting in an annual CO minimum during the Asian summer monsoon (Fig. 8). The CO-rich air masses for the surface are uplifted in the upper troposphere due to deep convection over the area (Sect. 3.1.2).

As for CO, O_3 seasonality is also linked with the seasonality of the meteorological conditions and dynamics over Asia. The O_3 maximum in April is attributed to the intense solar radiation associated with important amount of precursors from mostly AN emissions, except for South China where BB emissions dominate. The O_3 minimum occurs during the Asian summer monsoon (July), because of lower O_3 production in the presence of convective clouds relative to clear sky conditions (Sect. 3.1.2).

Despite the CO emissions reductions over South China, the O_3 levels remain relatively high (Fig. 8a). This is because the O_3 production regime over South China is VOCs-limited (Li et al., 2013), and the total NMVOCs emissions increased by a factor of 3.5 (1997–2017) because of activity increases in the solvent, energy, and industry sectors (Zheng et al., 2018a). Despite the successful controls of NO_x emissions from coal fired power plants since 2010 over Eastern China (Wang et al., 2017), it is recommended to apply controls over VOCs emissions as they control the local O_3 distribution. In contrast, over India the O_3 production regime is NO_x-limited (Kumar et al., 2012), as the local emissions are mostly associated with incomplete combustion proccesses by biofuel burning, and thus higher NMHC to NO_x emission ratio as compared to other regions of the Northern Hemisphere (Lawrence and Lelieveld, 2010).

Concerning Central Africa, the O_3 and CO maximum in the LT during the dry season, indicates the strong dependence of the CO and O_3 distribution on the surface emissions, as over NT Africa. The CO magnitude over Central Africa is similar to the one over Sahel and Guinea Gulf during the respective dry season, even though the emissions rates are higher over the former (Table 2). This is because higher amount of CO impacted by the Southern Hemisphere African fires is transported towards the NT Africa due to the trade winds, relative to the respective southward transport during the Northern Hemisphere dry season (Fig. 9). In addition, the O_3 mixing ratio is slightly higher over Central Africa (85 ppb) likely indicating rapid photochemical O_3 production by BB precursors (Singh et al., 1996) during the Southern Hemisphere fires.

The smallest LT CO maximum over the NT are observed over Arabia and East Africa clusters and South America (Fig. 8) because of the smallest emissions rates among the tropics (Table 2). The CO emissions over Middle East are mainly related to electricity generation, water desalination, and industry supplied by oil and gas deposits with cheap but relatively clean fuels

(Krotkov et al., 2016). In addition, because of its location between the two highest emittors (Asia and Africa), transport plays a significant role in CO enhancements over AEA, especially in the MT and UT where long range transport of emissions is favoured (Figs. 9 panels 1 b–c; 2 a–c and 2b–c). This transport from Asia and Africa over AEA clusters determines the O_3 maxima over the AEA clusters (Sect. 3.1.4). Similarly, over NT South America, the local AN contributions are much smaller than the respective local Asian of African ones, indicating lower pollution levels over South America than Asia and Africa. The O_3 maximum is controlled by $LiNO_x$ emissions at higher altitudes.

From the previous analysis, all the tropical clusters and the associated CO source regions exhibit primarily local influence, in the proximity of the region where they are emitted. However, CO transport plays also an important role in the CO distribution over the tropics. CO sources located over Africa show the maximum influence on the regional tropical CO. The highest impact of the African emissions is found at an inter-hemispheric scale, where CO from the dry-season African regions is transported towards the wet-season African (Fig. 9 panels 1 and 2). As a result, CO contributions of 45–50 ppb (resp. over 50 ppb) from Northern Hemisphere (resp. Southern Hemisphere) Africa is found over Southern (resp. Northern) Africa during the respective dry season in the LT and MT. Also, Northern Hemisphere African emissions are transported towards South America (10–15 ppb in MT; 5–10 ppb in the rest) in April (Fig. not shown) and significantly contribute to the local South American annual maximum (30 % and 50 % of CO anomalies over Caracas (LT and MT resp.) (Fig. 4a–b).

During the transport of the Southern (resp. Northern) Hemisphere African emissions towards the ITCZ location in the Northern (resp. Southern) Africa, the air masses reach convective regions and are injected in the UT_{cruise} (Fig. 10). This explains why the Southern (resp. Northern) Hemisphere African emissions are dominant in the wet-season hemisphere during July (resp. January) (Figs. 10 and resp. A6 and A4). Nevertheless, the Northern Hemisphere African contribution in the UT_{cruise} CO anomalies is present on a local scale all year long, above NT Africa and South Atlantic. During the dry season, the impact of the Northern Hemisphere African emissions is stronger and extends to a wider area over South America, Middle East, South Asia (Figs. A4 NHAF).

The contribution of Asian emissions in the tropical LT is limited to a regional or local scale, as they are mostly impact neighbour Asian regions (Fig. 9a)(see Sect. 3.1.2 for more details). CO export from Asia is favoured during the Asian summer monsoon and post monsoon (July and October) in the UT, where the transport is favoured due to stronger winds relative to the surface (Fig. S3).

During the Asian summer monsoon, the CO-rich (and O_3-poor) air masses from the boundary layer (Fig. 2c and g) are convectively uplifted in the UT_{cruise} (Figs. 10c and A6), and trapped in the AMA circulation (see Sect. 3.1.2). Asian emissions are transported towards Arabia (25–30 ppb) and Eastern Africa (10–15 ppb) in the UT_{cruise} (Figs. 10c; 9 panel 3c and A6 SEAS and CEAS). Subsidence of air masses from AMA above Arabia are responsible for an O_3 maximum above AEA (Fig. 8a) (Sect. 3.1.4). During the post monsoon season (October), sporadic convection uplifts CO emitted by the Equatorial Asian fires in the UT_{cruise} (Figs. 10g, A7 EQAS) (see Sect. 3.1.2). At the same time, convection over continental Asia uplifts SouthEast Asian AN emissions (Figs. 10d and A7 SEAS) in the UT_{cruise}. As a result, CO from the Asian emissions impacts CO anomalies in the UT over Eastern Africa (15–20 ppb from Equatorial Asia and 5–10 ppb from SouthEast Asia; Fig. not shown).

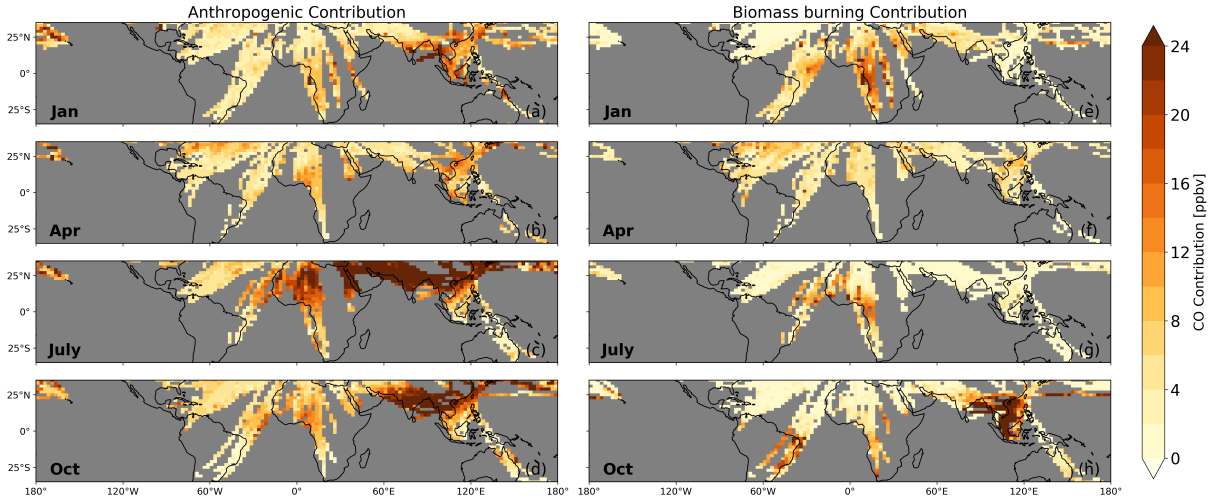

Figure 10. Mean AN (a–d) and BB (e–h) contributions in ppb between 300–185 hPa from 2002–2019.

4 Summary and conclusions

IAGOS O_3 and CO observations since 1994 and 2002 respectively, were used (when available) in order to analyse vertical profiles over 20 tropical sites, along with the UT_{cruise}. One limitation of our study is the rather limited spatial coverage of IAGOS profiles to limited locations. However, according to Petetin et al. (2018a), a few hundreds meters above the ground, these measurements are representative of the urban background and of the regional scale at higher altitudes in the lower troposphere. Furthermore, IASI, which provides global daily O_3 and CO distributions with a coarse vertical resolution, allows us to complement IAGOS observations on the global scale over the data sparse tropical band. Throughout the paper we have shown that the anomalies detected by IAGOS are often also detected by IASI at the regional scale.

In the LT, the CO anomalies are caused by a combination of AN and BB emissions. In the majority of the clusters, local AN contributions are dominant all year long. The BB contribution increases or dominates over some clusters, when the regional or local fires are active. Local AN emissions have greatest impact over Asia where they account for more than 80 % of the CO. The BB impact increases over South China (35 % in April), and dominates over the Gulf of Thailand (90 % in October) during the local fires (SouthEast and Equatorial Asian resp.). Over NH NT Africa, with contributions in the range of 57-85% local AN emissions largely dominate the CO anomalies all year long. There are a few exceptions of larger BB contributions in January over Guinea Gulf (53%) and in July over Lagos (53%) and Guinea Gulf (66%) during Northern and Southern Hemisphere African BB seasons. Similar impact of the Southern Hemisphere African fires is found over Khartoum in July. In contrast, the rest of the AEA clusters are impacted by local AN emissions all year long (70–95 %). Over South America, stronger local AN contribution are found over the ST (81–94 % over SBrazil) than in the NT (75–80 % Caracas and Bogota), while the BB contributions are similar (51 % over Caracas in April and 53 % over SBrazil in October). The highest BB impact is found over ST Africa all year long (57%–90%), except in April, with BB emissions mostly originating from local fires, but

also from Northern Hemisphere Africa in January (45-73%) and Southern Hemisphere Southern America in October (29% over Windhoek). During the transition periods, the local AN contributions are larger (46 and 80 %). Our results highlight the importance of the AN emissions over the tropical sites, even in the ST. This is in accordance with the global decreasing trends of BB and the increasing AN emissions.

In the MT and UT, the BB contributions are increased compared to the LT, and their effect dominates over more clusters. Also, the contribution of the transport is more important than in the LT, where mostly local emissions dominate. Over NT Africa, the BB dominates twice a year, during the Northern and Southern Hemisphere dry seasons, because of local and Southern Hemisphere African fires respectively. In NT Africa, as in the LT, BB dominates all year long except April. In addition to the African BB, AN SouthEast Asian and BB Southern Hemisphere South American contributions are found in the MT and UT. Over Asia, SouthEast Asian BB contributions dominate over the South East Asian coast (South China, Manila, Ho Chi Minh City) in April in the MT. In contrast, the impact of the Equatorial Asian BB is stronger in the UT, and has a largest spatial extent over the South East Asian coast (China, Ho Chi Minh City, Manila), India (Madras) and Eastern Africa (Addis Ababa).

Over Africa, the O_3 and CO maxima are observed in the LT during the respective dry season. The role of the local AN emissions are more important than previously documented as: i) local AN emissions control the CO anomalies over Lagos and Sahel, and ii) the persistent CO-rich surface layer in Central Africa is caused by local AN emissions (40 and 86 %) in the absence of local fires. Africa is also the most important tropical region in terms of export of emissions in the tropical troposphere. According to IASI, the main export pathway is the inter-hemispheric transport of O_3 and precursors from the dry-season African regions to the wet-season ones ($\approx$ 50 ppb), confirmed by SOFT-IO. During the dry season, the Northern (resp. Southern) Hemisphere African fires are the dominant source of CO over AEA (resp. Khartoum and Jeddah) in the MT and UT, and they also reach India accounting for 5–10 ppb in the MT and UT. Transport of mostly BB emissions from Africa occurs all year round towards northern South America in all tropospheric layers. The highest Northern Hemisphere African regional impact is found over Caracas in the MT and UT (30 % on average). In contrast, the impact of Asian emissions, is mostly limited on a regional or local scale, especially in the LT and MT. The transport of the Asian emissions is important only during the Asian summer monsoon in the UT towards Arabia and Eastern Africa.

The highest O_3 and CO maxima among the tropical clusters occur in the LT of NT Africa in January (75 ppb at 2.5 km for O_3 and 800 ppb at 0.3 km for CO over Lagos). This is largely a result of the local AN emissions as suggested by the co-occurrence of the peaks of O_3 and CO in the LT. In contrast over Asia, the second most polluted region, the distributions are mostly controlled by meteorological conditions associated with the Asian monsoon phase. The CO maximum occurs in the LT during January, due to the stability of the northeasterlies which confine the CO-rich air masses to the LT. The annual maximum of O_3 occurs during the pre monsoon season (April) when the increased solar radiation favours O_3 production. During the Asian summer monsoon, O_3 and CO mixing ratio minimize in the LT because of : i) transport of clean oceanic air above continental Asia, ii) reduced photochemical O_3 production due to cloudy conditions, and iii) convective uplift of CO-rich air masses from the surface towards the Asian upper troposphere.

Over Asia, the LT and MT CO and O_3 anomalies are mostly impacted by regional or local Asian emissions of AN origin. The BB contribution is important during April and significantly contributes to CO anomalies over South China. According to IASI, the BB impact extends over the tropical Pacific. The export of the AN Asian emissions is important only in the UT during the Asian summer monsoon and post monsoon season (July and October). According to IASI, the polluted air masses from the surface are uplifted in the UT_{cruise} in July and are trapped in the AMA. These air masses are transported over AEA (CO contributions of 25–30 ppb and 10–15 ppb) causing the annual O_3 maxima due to subsidence and high isolation over the regions. This highlights the importance of long range transport for the air quality in the UT over Arabia, which shows the lowest CO local contribution and the highest O_3 levels among the tropical clusters. The CO transport towards Eastern Africa in the UT by the Tropical Easterly Jet, is found in October when the air masses impacted by the Indonesian fires, and the AN continental source are uplifted in the UT, and transported towards Eastern Africa (CO contributions of 15–20 ppb and 5–10 ppb respectively).

Last, over South America the local CO contributions at the surface level are as low as over Arabia and Eastern Asia. During the dry season (October), when the convection moves over the South American fires, CO and precursors are trapped in an anticyclonic circulation developed over Central South America, resulting in the annual local maxima of O_3 and CO. The transport of O_3 and precursors over Atlantic can be seen by IASI and this contributes to the O_3 wave-one pattern. This is confirmed by SOFT-IO which calculates Northern and Southern Hemisphere South American contribution of 10–15 ppb each towards Windhoek, in the altitude of the anticyclone (MT).

Appendix A: SOFT-IO CO contributions

A1 Vertical profiles

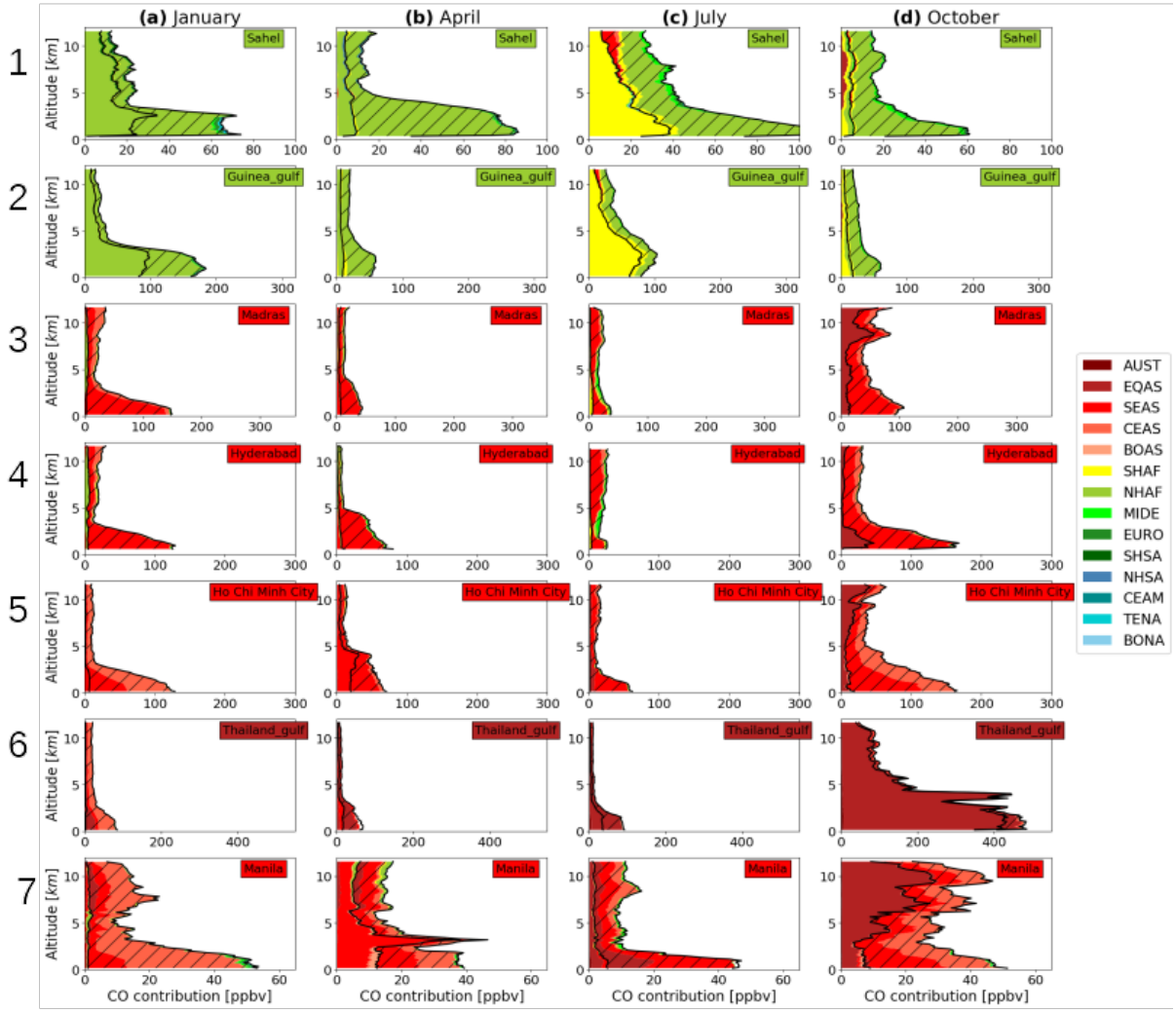

Figure A1. Same as Fig. 3 (panel 3) for CO contributions over Sahel (1), Gulf of Guinea (2), Madras (3), Hyderabad (4), Ho Chi Minh City (5), Gulf of Thailand (6) and Manila (7).

A1 Low, mid and upper troposphere

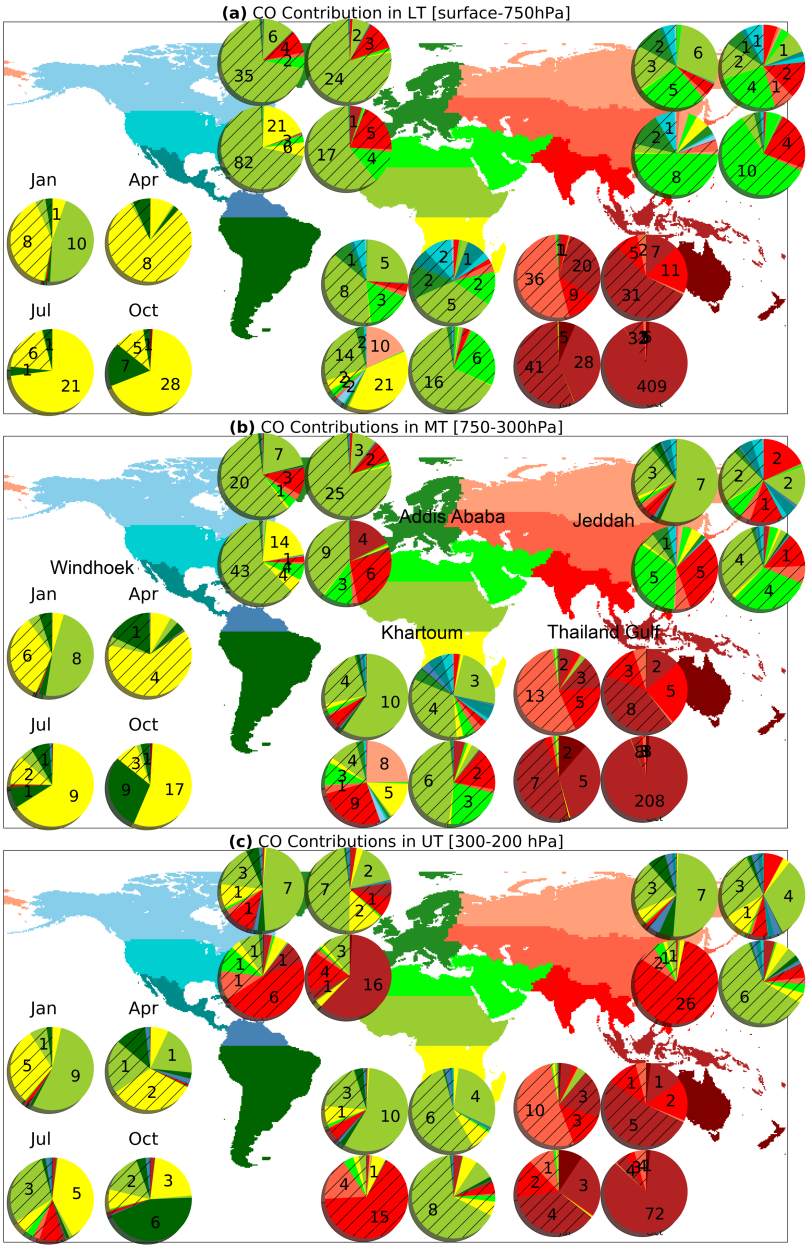

Figure A2. Same as Fig. 4 for CO contributions over Windhoek, Addis Ababa, Khartoum, Jeddah and Gulf of Thailand.

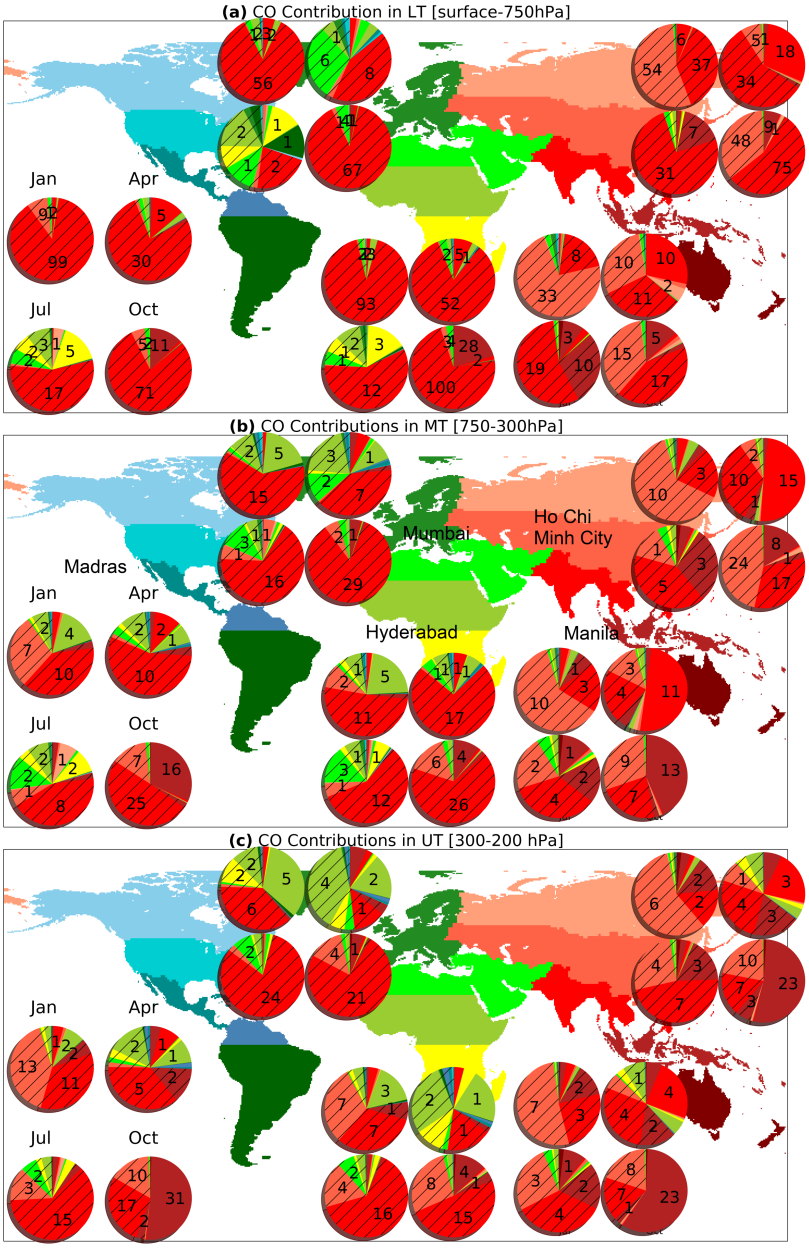

Figure A3. Same as Fig. 4 for CO contributions over Madras, Mumbai, Hyderabad, Ho Chi Minh City and Manila.

A2 Upper troposphere

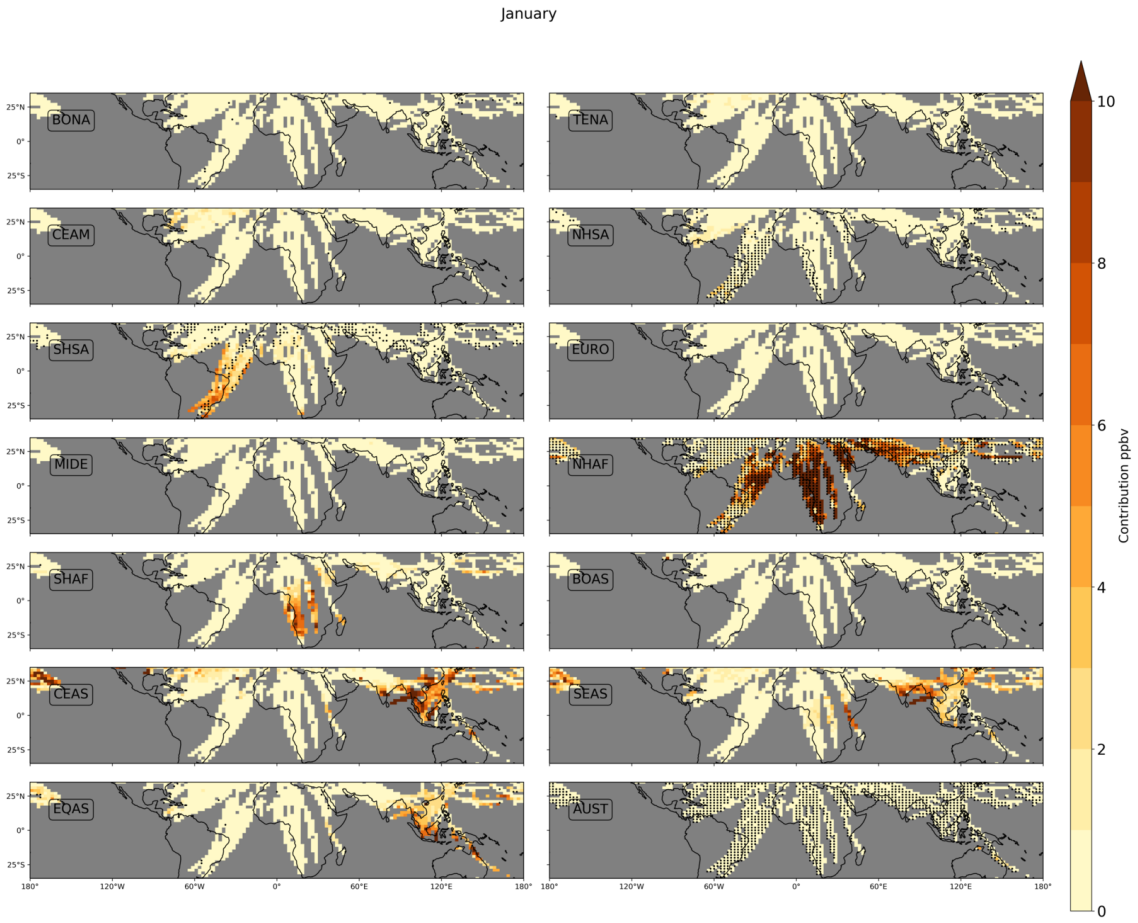

Figure A4. Mean CO contribution (in ppb) per source region in the tropical UT$_{cruise}$ (300–185 hPa) averaged from 2002–2020 for January. The hatched part indicates BB as the dominant source of CO.

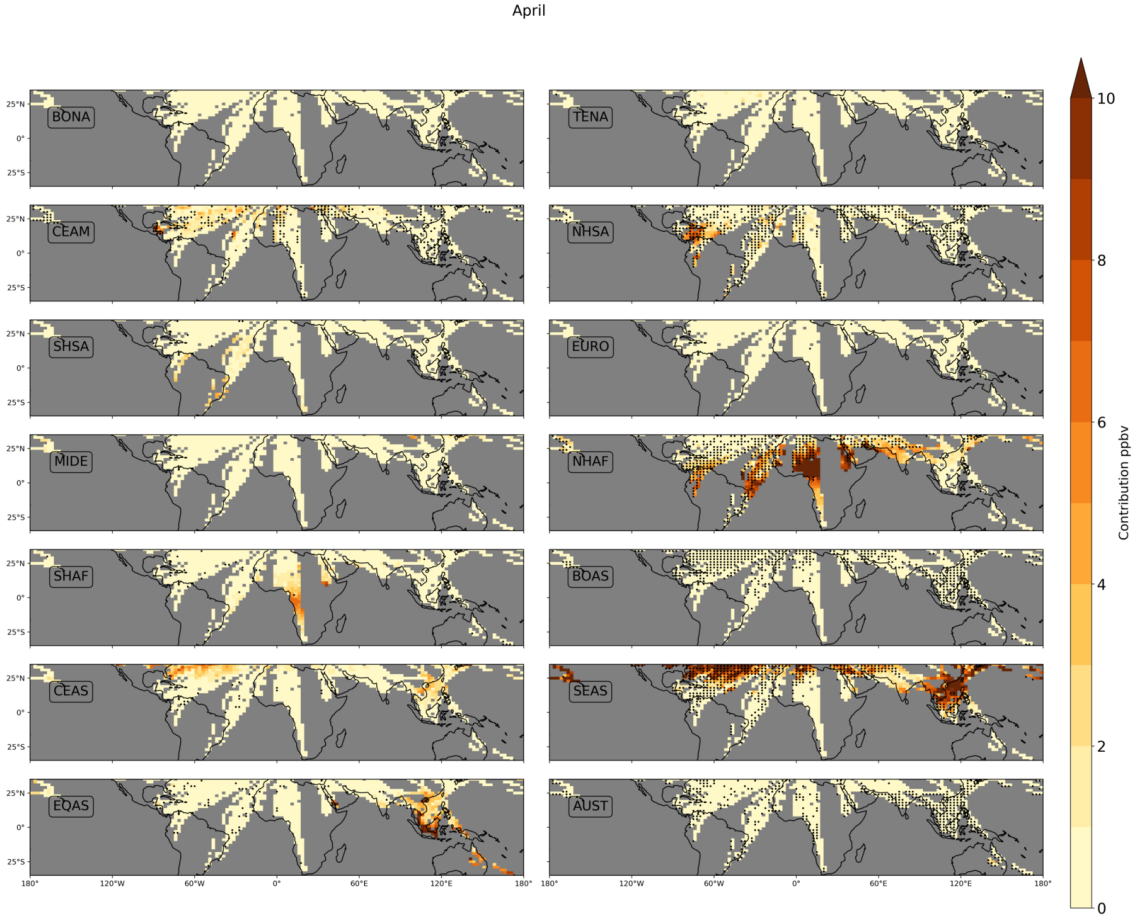

Figure A5. Same as Fig. A4 for April.

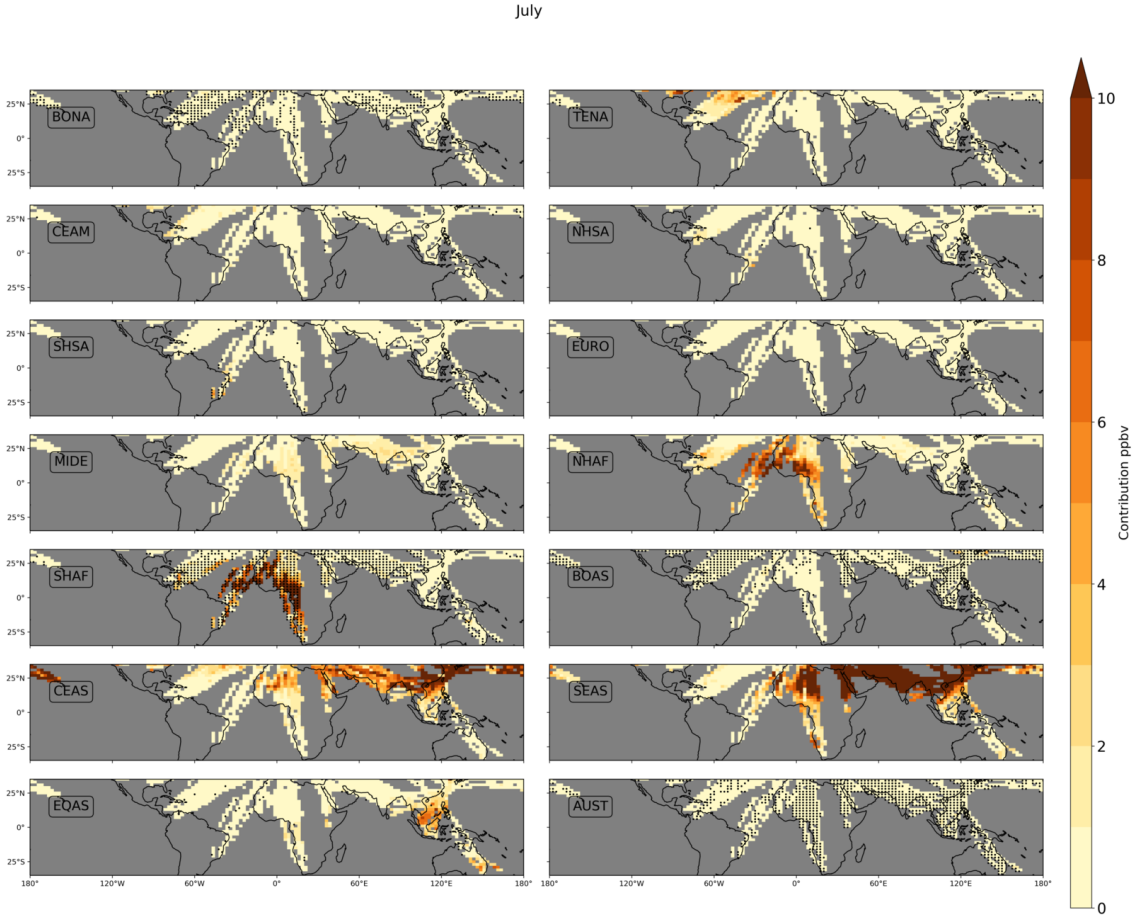

Figure A6. Same as Fig. A4 for July.

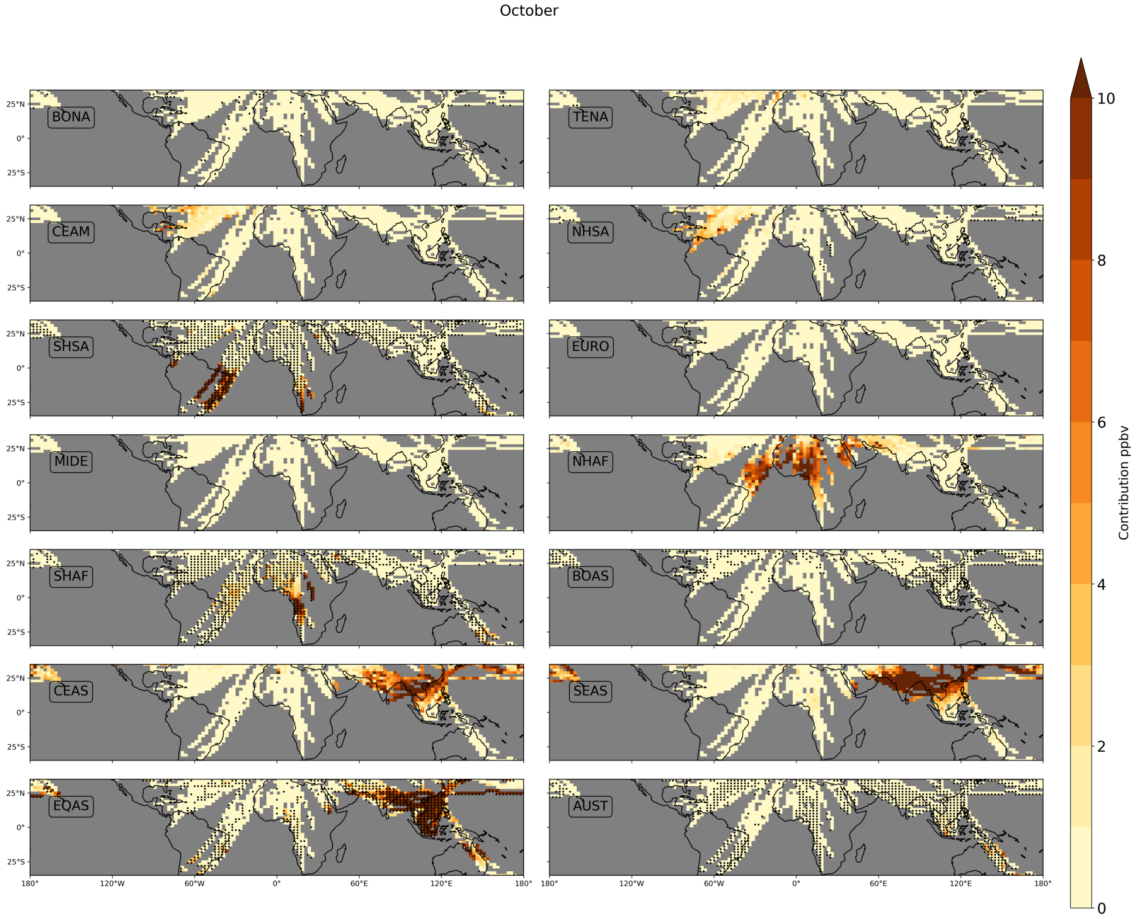

Figure A7. Same as Fig. A4 for October.

Data availability. The IAGOS data are available on the IAGOS data portal (https://doi.org/10.25326/20). The SOFT-IO v1.0 products are part of the ancillary products of IAGOS central database (https://doi.org/10.25326/2; https://doi.org/10.25326/3). The SOFRID-O_3 data are freely available on the IASI-SOFRID website (http://thredds.sedoo.fr/iasi-sofrid-o3-co/, last access: 8 June 2022; SEDOO, 2014).

Author contributions. MT, BS and BB designed the research. All the co-authors contributed to acquisition of data. MT analysed the data. MT, BS and BB interpreted the data. MT drafted the article. MT, BS and BB revised the article. VT and HC commented the article. ELF and BB are responsible for the SOFRID retrieval software. ELF is in charge of the production and quality control of SOFRID data.

Competing interests. The authors declare that they have no conflict of interest.

Acknowledgements. We acknowledge the strong support of the European Commission, Airbus and the airlines (Deutsche Lufthansa, Air France, Austrian, Air Namimbia, Cathay Pacific, Iberia, China Airlines and Hawaiian Airlines) that have carried the MOZAIC or IAGOS equipment and performed the maintenance since 1994. IAGOS has been funded by the European Union projects IAGOS–DS and IAGOS–ERI. Additionally, IAGOS has been funded by INSU-CNRS (France), Météo-France, Université Paul Sabatier (Toulouse, France) and Research Center Jülich (FZJ, Jülich, Germany). The IAGOS database is supported in France by AERIS (https://www.aeris-data.fr). IASI is a joint mission of EUMETSAT and the Centre National d'Etudes Spatiales (CNES, France). The authors acknowledge the CNES for financial support for the IASI activities.

Financial support. This research has been supported by Bonus Stratégique programme at Université Paul Sabatier Toulouse III who funded the first author's doctoral position.

References

Adon, M., Galy-Lacaux, C., Yoboué, V., Delon, C., Lacaux, J., Castera, P., Gardrat, E., Pienaar, J., Al Ourabi, H., Laouali, D., et al.: Long term measurements of sulfur dioxide, nitrogen dioxide, ammonia, nitric acid and ozone in Africa using passive samplers, Atmospheric Chemistry and Physics, 10, 7467–7487, https://doi.org/10.5194/acp-10-7467-2010, 2010.

Adon, M., Yoboué, V., Galy-Lacaux, C., Liousse, C., Diop, B., Gardrat, E., Ndiaye, S. A., Jarnot, C., et al.: Measurements of NO2, SO2, NH3, HNO3 and O3 in West African urban environments, Atmospheric Environment, 135, 31–40, https://doi.org/10.1016/j.atmosenv.2016.03.050, 2016.

Aghedo, A. M., Schultz, M. G., and Rast, S.: The influence of African air pollution on regional and global tropospheric ozone, Atmospheric Chemistry and Physics, 7, 1193–1212, https://doi.org/10.1016/j.atmosenv.2016.03.050, 2007.

Alonso, M. F., Longo, K. M., Freitas, S. R., da Fonseca, R. M., Marécal, V., Pirre, M., and Klenner, L. G.: An urban emissions inventory for South America and its application in numerical modeling of atmospheric chemical composition at local and regional scales, Atmospheric Environment, 44, 5072–5083, https://doi.org/10.1016/j.atmosenv.2010.09.013, 2010.

Andela, N., Morton, D. C., Giglio, L., Chen, Y., van der Werf, G. R., Kasibhatla, P. S., DeFries, R. S., Collatz, G., Hantson, S., Kloster, S., et al.: A human-driven decline in global burned area, Science, 356, 1356–1362, https://doi.org/10.1126/science.aal4108, 2017.

Archibald, A., Neu, J., Elshorbany, Y., Cooper, O., Young, P., Akiyoshi, H., Cox, R., Coyle, M., Derwent, R., Deushi, M., et al.: Tropospheric Ozone Assessment ReportA critical review of changes in the tropospheric ozone burden and budget from 1850 to 2100, Elementa: Science of the Anthropocene, 8, https://doi.org/10.1525/elementa.2020.034, 2020.

Assamoi, E.-M. and Liousse, C.: A new inventory for two-wheel vehicle emissions in West Africa for 2002, Atmospheric Environment, 44, 3985–3996, https://doi.org/10.1016/j.atmosenv.2010.06.048, 2010.

Barret, B., Ricaud, P., Mari, C., Attié, J.-L., Bousserez, N., Josse, B., Le Flochmoën, E., Livesey, N., Massart, S., Peuch, V.-H., et al.: Transport pathways of CO in the African upper troposphere during the monsoon season: a study based upon the assimilation of spaceborne observations, Atmospheric Chemistry and Physics, 8, 3231–3246, https://doi.org/10.5194/acp-8-3231-2008, 2008.

Barret, B., Williams, J., Bouarar, I., Yang, X., Josse, B., Law, K., Pham, M., Le Flochmoën, E., Liousse, C., Peuch, V., et al.: Impact of West African Monsoon convective transport and lightning NO x production upon the upper tropospheric composition: a multi-model study, Atmospheric Chemistry and Physics, 10, 5719–5738, https://doi.org/10.5194/acp-10-5719-2010, 2010.

Barret, B., Le Flochmoen, E., Sauvage, B., Pavelin, E., Matricardi, M., and Cammas, J.-P.: The detection of post-monsoon tropospheric ozone variability over south Asia using IASI data, Atmospheric Chemistry and Physics, 11, 9533–9548, https://doi.org/10.5194/acp-11-9533-2011, 2011.

Barret, B., Sauvage, B., Bennouna, Y., and Le Flochmoen, E.: Upper-tropospheric CO and O 3 budget during the Asian summer monsoon, Atmospheric Chemistry and Physics, 16, 9129–9147, https://doi.org/10.5194/acp-16-9129-2016, 2016.

Barret, B., Emili, E., and Le Flochmoen, E.: A tropopause-related climatological a priori profile for IASI-SOFRID ozone retrievals: improvements and validation, Atmospheric Measurement Techniques, 13, 5237–5257, https://doi.org/10.5194/amt-13-5237-2020, 2020.

Barret, B., Gouzenes, Y., Le Flochmoen, E., and Ferrant, S.: Retrieval of Metop-A/IASI N2O profiles and validation with NDACC FTIR data, Atmosphere, 12, 219, https://doi.org/10.3390/atmos12020219, 2021.

Blot, R., Nedelec, P., Boulanger, D., Wolff, P., Sauvage, B., Cousin, J.-M., Athier, G., Zahn, A., Obersteiner, F., Scharffe, D., et al.: Internal consistency of the IAGOS ozone and carbon monoxide measurements for the last 25 years, Atmospheric Measurement Techniques, 14, 3935–3951, https://doi.org/10.5194/amt-14-3935-2021, 2021.

Bourgeois, I., Peischl, J., Thompson, C. R., Aikin, K. C., Campos, T., Clark, H., Commane, R., Daube, B., Diskin, G. W., Elkins, J. W., et al.: Global-scale distribution of ozone in the remote troposphere from the ATom and HIPPO airborne field missions, Atmospheric Chemistry and Physics, 20, 10 611–10 635, https://doi.org/10.5194/acp-20-10611-2020, 2020.

Bourgeois, I., Peischl, J., Neuman, J. A., Brown, S. S., Thompson, C. R., Aikin, K. C., Allen, H. M., Angot, H., Apel, E. C., Baublitz, C. B., et al.: Large contribution of biomass burning emissions to ozone throughout the global remote troposphere, Proceedings of the National Academy of Sciences, 118, e2109628 118, https://doi.org/10.1073/pnas.2109628118, 2021.

Boynard, A., Hurtmans, D., Koukouli, M. E., Goutail, F., Bureau, J., Safieddine, S., Lerot, C., Hadji-Lazaro, J., Wespes, C., Pommereau, J.-P., et al.: Seven years of IASI ozone retrievals from FORLI: validation with independent total column and vertical profile measurements, Atmospheric Measurement Techniques, 9, 4327–4353, https://doi.org/10.5194/amt-9-4327-2016, 2016.

Boynard, A., Hurtmans, D., Garane, K., Goutail, F., Hadji-Lazaro, J., Koukouli, M. E., Wespes, C., Vigouroux, C., Keppens, A., Pommereau, J.-P., et al.: Validation of the IASI FORLI/EUMETSAT ozone products using satellite (GOME-2), ground-based (Brewer–Dobson, SAOZ, FTIR) and ozonesonde measurements, Atmospheric Measurement Techniques, 11, 5125–5152, https://doi.org/10.5194/amt-11-5125-2018, 2018.

Buchholz, R. R., Worden, H. M., Park, M., Francis, G., Deeter, M. N., Edwards, D. P., Emmons, L. K., Gaubert, B., Gille, J., Martínez-Alonso, S., et al.: Air pollution trends measured from Terra: CO and AOD over industrial, fire-prone, and background regions, Remote Sensing of Environment, 256, 112 275, https://doi.org/10.1016/j.rse.2020.112275, 2021.

Clerbaux, C., Boynard, A., Clarisse, L., George, M., Hadji-Lazaro, J., Herbin, H., Hurtmans, D., Pommier, M., Razavi, A., Turquety, S., et al.: Monitoring of atmospheric composition using the thermal infrared IASI/MetOp sounder, Atmospheric Chemistry and Physics, 9, 6041–6054, https://doi.org/10.5194/acp-9-6041-2009, 2009.

Cohen, Y., Petetin, H., Thouret, V., Marécal, V., Josse, B., Clark, H., Sauvage, B., Fontaine, A., Athier, G., Blot, R., et al.: Climatology and long-term evolution of ozone and carbon monoxide in the upper troposphere–lower stratosphere (UTLS) at northern midlatitudes, as seen by IAGOS from 1995 to 2013, Atmospheric Chemistry and Physics, 18, 5415–5453, https://doi.org/10.5194/acp-18-5415-2018, 2018.

Cros, B., Delon, C., Affre, C., Marion, T., Druilhet, A., Perros, P., and Lopez, A.: Sources and sinks of ozone in savanna and forest areas during EXPRESSO: Airborne turbulent flux measurements, Journal of Geophysical Research: Atmospheres, 105, 29 347–29 358, https://doi.org/10.1029/2000JD900451, 2000.

Curtis, L., Rea, W., Smith-Willis, P., Fenyves, E., and Pan, Y.: Adverse health effects of outdoor air pollutants, Environment international, 32, 815–830, https://doi.org/10.1016/j.envint.2006.03.012, 2006.

Cussac, M., Marécal, V., Thouret, V., Josse, B., and Sauvage, B.: The impact of biomass burning on upper tropospheric carbon monoxide: a study using MOCAGE global model and IAGOS airborne data, Atmospheric Chemistry and Physics, 20, 9393–9417, https://doi.org/10.5194/acp-20-9393-2020, 2020.

De Wachter, E., Barret, B., Le Flochmoën, E., Pavelin, E., Matricardi, M., Clerbaux, C., Hadji-Lazaro, J., George, M., Hurtmans, D., Coheur, P.-F., et al.: Retrieval of MetOp-A/IASI CO profiles and validation with MOZAIC data, Atmospheric Measurement Techniques, 5, 2843–2857, https://doi.org/10.5194/amt-5-2843-2012, 2012.

Deeter, M., Martínez-Alonso, S., Andreae, M. O., and Schlager, H.: Satellite-based analysis of CO seasonal and interannual variability over the Amazon Basin, Journal of Geophysical Research: Atmospheres, 123, 5641–5656, https://doi.org/10.1029/2018JD028425, 2018.

Dufour, G., Eremenko, M., Orphal, J., and Flaud, J.-M.: IASI observations of seasonal and day-to-day variations of tropospheric ozone over three highly populated areas of China: Beijing, Shanghai, and Hong Kong, Atmospheric Chemistry and Physics, 10, 3787–3801, https://doi.org/10.5194/acp-10-3787-2010, 2010.

Duncan, B. N., Lamsal, L. N., Thompson, A. M., Yoshida, Y., Lu, Z., Streets, D. G., Hurwitz, M. M., and Pickering, K. E.: A space-based, high-resolution view of notable changes in urban NOx pollution around the world (2005–2014), Journal of Geophysical Research: Atmospheres, 121, 976–996, https://doi.org/10.1002/2015JD024121, 2016.

Edwards, D., Emmons, L., Gille, J., Chu, A., Attié, J.-L., Giglio, L., Wood, S., Haywood, J., Deeter, M., Massie, S., et al.: Satellite-observed pollution from Southern Hemisphere biomass burning, Journal of Geophysical Research: Atmospheres, 111, https://doi.org/10.1029/2005JD006655, 2006.

Emmons, L. K., Walters, S., Hess, P. G., Lamarque, J.-F., Pfister, G. G., Fillmore, D., Granier, C., Guenther, A., Kinnison, D., Laepple, T., et al.: Description and evaluation of the Model for Ozone and Related chemical Tracers, version 4 (MOZART-4), Geoscientific Model Development, 3, 43–67, https://doi.org/10.5194/gmd-3-43-2010, 2010.

Eremenko, M., Dufour, G., Foret, G., Keim, C., Orphal, J., Beekmann, M., Bergametti, G., and Flaud, J.-M.: Tropospheric ozone distributions over Europe during the heat wave in July 2007 observed from infrared nadir spectra recorded by IASI, Geophysical Research Letters, 35, https://doi.org/10.1029/2008GL034803, 2008.

Galanter, M., Levy, H., and Carmichael, G. R.: Impacts of biomass burning on tropospheric CO, NO x, and O3, Journal of Geophysical Research: Atmospheres, 105, 6633–6653, https://doi.org/10.1029/1999JD901113, 2000.

Gaudel, A., Cooper, O. R., Ancellet, G., Barret, B., Boynard, A., Burrows, J., Clerbaux, C., Coheur, P.-F., Cuesta, J., Cuevas, E., et al.: Tropospheric Ozone Assessment Report: Present-day distribution and trends of tropospheric ozone relevant to climate and global atmospheric chemistry model evaluation, Elementa: science of the anthropocene, 6, https://doi.org/10.1525/elementa.291, 2018.

Gaudel, A., Cooper, O. R., Chang, K.-L., Bourgeois, I., Ziemke, J. R., Strode, S. A., Oman, L. D., Sellitto, P., Nédélec, P., Blot, R., et al.: Aircraft observations since the 1990s reveal increases of tropospheric ozone at multiple locations across the Northern Hemisphere, Science Advances, 6, eaba8272, https://doi.org/10.1525/elementa.291, 2020.

Gauss, M., Myhre, G., Pitari, G., Prather, M., Isaksen, I., Berntsen, T., Brasseur, G., Dentener, F., Derwent, R., Hauglustaine, D., et al.: M uller, JF, Plantevin, P., Pyle, JA, Rogers, HL, Stevenson, DS, Sundet, JK, van Weele, M., and Wild, O.: Radiative forcing in the 21st century due to ozone changes in the troposphere and the lower stratosphere, J. Geophys. Res, 108, https://doi.org/10.1029/2002JD002624, 2003.

George, M., Clerbaux, C., Hurtmans, D., Turquety, S., Coheur, P.-F., Pommier, M., Hadji-Lazaro, J., Edwards, D., Worden, H., Luo, M., et al.: Carbon monoxide distributions from the IASI/METOP mission: evaluation with other space-borne remote sensors, Atmospheric Chemistry and Physics, 9, 8317–8330, https://doi.org/10.5194/acp-9-8317-2009, 2009.

Granier, C., Bessagnet, B., Bond, T., D'Angiola, A., Denier van der Gon, H., Frost, G. J., Heil, A., Kaiser, J. W., Kinne, S., Klimont, Z., et al.: Evolution of anthropogenic and biomass burning emissions of air pollutants at global and regional scales during the 1980–2010 period, Climatic change, 109, 163–190, https://doi.org/10.1007/s10584-011-0154-1, 2011.

Gressent, A., Sauvage, B., Defer, E., Pätz, H. W., Thomas, K., Holle, R., Cammas, J.-P., Nédélec, P., Boulanger, D., Thouret, V., et al.: Lightning NOx influence on large-scale NOy and O3 plumes observed over the northern mid-latitudes, Tellus B: Chemical and Physical Meteorology, 66, 25 544, https://doi.org/10.3402/tellusb.v66.25544, 2014.

Gressent, A., Sauvage, B., Cariolle, D., Evans, M., Leriche, M., Mari, C., and Thouret, V.: Modeling lightning-NO x chemistry on a sub-grid scale in a global chemical transport model, Atmospheric Chemistry and Physics, 16, 5867–5889, https://doi.org/10.5194/acp-16-5867-2016, 2016.

Hedelius, J. K., Toon, G. C., Buchholz, R. R., Iraci, L. T., Podolske, J. R., Roehl, C. M., Wennberg, P. O., Worden, H. M., and Wunch, D.: Regional and urban column CO trends and anomalies as observed by MOPITT over 16 years, Journal of Geophysical Research: Atmospheres, 126, e2020JD033 967, https://doi.org/10.1029/2020JD033967, 2021.

Heue, K.-P., Coldewey-Egbers, M., Delcloo, A., Lerot, C., Loyola, D., Valks, P., and Van Roozendael, M.: Trends of tropical tropospheric ozone from 20 years of European satellite measurements and perspectives for the Sentinel-5 Precursor, Atmospheric Measurement Techniques, 9, 5037–5051, https://doi.org/10.5194/amt-9-5037-2016, 2016.

IPCC: Climate change 2021: The physical science basis, Tech. rep., http://www.ipcc.ch/report/ar6/wg1/, 2021.

Jacob, D. J., Heikes, E., Fan, S.-M., Logan, J. A., Mauzerall, D., Bradshaw, J., Singh, H., Gregory, G., Talbot, R., Blake, D., et al.: Origin of ozone and NOx in the tropical troposphere: A photochemical analysis of aircraft observations over the South Atlantic basin, Journal of Geophysical Research: Atmospheres, 101, 24 235–24 250, https://doi.org/10.1029/96JD00336, 1996.

Jaeglé, L., Martin, R., Chance, K., Steinberger, L., Kurosu, T., Jacob, D. J., Modi, A., Yoboué, V., Sigha-Nkamdjou, L., and Galy-Lacaux, C.: Satellite mapping of rain-induced nitric oxide emissions from soils, Journal of Geophysical Research: Atmospheres, 109, https://doi.org/10.1029/2004JD004787, 2004.

Jerrett, M., Burnett, R. T., Pope III, C. A., Ito, K., Thurston, G., Krewski, D., Shi, Y., Calle, E., and Thun, M.: Long-term ozone exposure and mortality, New England Journal of Medicine, 360, 1085–1095, https://doi.org/10.1056/NEJMoa0803894, 2009.

Jia, J., Ladstätter-Weißenmayer, A., Hou, X., Rozanov, A., and Burrows, J. P.: Tropospheric ozone maxima observed over the Arabian Sea during the pre-monsoon, Atmospheric Chemistry and Physics, 17, 4915–4930, https://doi.org/10.5194/acp-17-4915-2017, 2017.

Kaiser, J., Heil, A., Andreae, M., Benedetti, A., Chubarova, N., Jones, L., Morcrette, J.-J., Razinger, M., Schultz, M., Suttie, M., et al.: Biomass burning emissions estimated with a global fire assimilation system based on observed fire radiative power, Biogeosciences, 9, 527–554, https://doi.org/10.5194/bg-9-527-2012, 2012.

Krotkov, N. A., McLinden, C. A., Li, C., Lamsal, L. N., Celarier, E. A., Marchenko, S. V., Swartz, W. H., Bucsela, E. J., Joiner, J., Duncan, B. N., et al.: Aura OMI observations of regional SO 2 and NO 2 pollution changes from 2005 to 2015, Atmospheric Chemistry and Physics, 16, 4605–4629, https://doi.org/10.5194/acp-16-4605-2016, 2016.

Kumar, R., Naja, M., Pfister, G., Barth, M., Wiedinmyer, C., and Brasseur, G.: Simulations over South Asia using the Weather Research and Forecasting model with Chemistry (WRF-Chem): chemistry evaluation and initial results, Geoscientific Model Development, 5, 619–648, https://doi.org/10.5194/gmd-5-619-2012, 2012.

Lamarque, J.-F., Bond, T. C., Eyring, V., Granier, C., Heil, A., Klimont, Z., Lee, D., Liousse, C., Mieville, A., Owen, B., et al.: Historical (1850–2000) gridded anthropogenic and biomass burning emissions of reactive gases and aerosols: methodology and application, Atmospheric Chemistry and Physics, 10, 7017–7039, https://doi.org/doi.org/10.5194/acp-10-7017-2010, 2010.

Lannuque, V., Sauvage, B., Barret, B., Clark, H., Athier, G., Boulanger, D., Cammas, J.-P., Cousin, J.-M., Fontaine, A., Le Flochmoën, E., et al.: Origins and characterization of CO and O 3 in the African upper troposphere, Atmospheric chemistry and physics, 21, 14 535–14 555, https://doi.org/10.5194/acp-21-14535-2021, 2021.

Lawrence, M. and Lelieveld, J.: Atmospheric pollutant outflow from southern Asia: a review, Atmospheric Chemistry and Physics, 10, 11 017–11 096, https://doi.org/10.5194/acp-10-11017-2010, 2010.

Lelieveld, J., Hoor, P., Jöckel, P., Pozzer, A., Hadjinicolaou, P., Cammas, J.-P., and Beirle, S.: Severe ozone air pollution in the Persian Gulf region, Atmospheric Chemistry and Physics, 9, 1393–1406, https://doi.org/10.5194/acp-9-1393-2009, 2009.

Lelieveld, J., Gromov, S., Pozzer, A., and Taraborrelli, D.: Global tropospheric hydroxyl distribution, budget and reactivity, Atmospheric Chemistry and Physics, 16, 12 477–12 493, https://doi.org/10.5194/acp-16-12477-2016, 2016.

Lelieveld, J. o., Crutzen, P., Ramanathan, V., Andreae, M., Brenninkmeijer, C., Campos, T., Cass, G., Dickerson, R., Fischer, H., De Gouw, J., et al.: The Indian Ocean experiment: widespread air pollution from South and Southeast Asia, Science, 291, 1031–1036, https://doi.org/10.1126/science.1057103, 2001.

Li, Y., Lau, A. K., Fung, J. C., Zheng, J., and Liu, S.: Importance of NOx control for peak ozone reduction in the Pearl River Delta region, Journal of Geophysical Research: Atmospheres, 118, 9428–9443, https://doi.org/10.1002/jgrd.50659, 2013.

Liu, J., Logan, J. A., Jones, D., Livesey, N., Megretskaia, I., Carouge, C., and Nedelec, P.: Analysis of CO in the tropical troposphere using Aura satellite data and the GEOS-Chem model: insights into transport characteristics of the GEOS meteorological products, Atmospheric Chemistry and Physics, 10, 12 207–12 232, https://doi.org/10.5194/acp-10-12207-2010, 2010.

Livesey, N., Logan, J., Santee, M., Waters, J., Doherty, R., Read, W., Froidevaux, L., and Jiang, J.: Interrelated variations of O 3, CO and deep convection in the tropical/subtropical upper troposphere observed by the Aura Microwave Limb Sounder (MLS) during 2004–2011, Atmospheric Chemistry and Physics, 13, 579–598, https://doi.org/10.5194/acp-13-579-2013, 2013.

Logan, J. A.: An analysis of ozonesonde data for the troposphere: Recommendations for testing 3-D models and development of a gridded climatology for tropospheric ozone, Journal of Geophysical Research: Atmospheres, 104, 16 115–16 149, https://doi.org/10.1029/1998JD100096, 1999.

Logan, J. A., Prather, M. J., Wofsy, S. C., and McElroy, M. B.: Tropospheric chemistry: A global perspective, Journal of Geophysical Research: Oceans, 86, 7210–7254, https://doi.org/10.1029/JC086iC08p07210, 1981.

Lu, X., Zhang, L., Zhao, Y., Jacob, D. J., Hu, Y., Hu, L., Gao, M., Liu, X., Petropavlovskikh, I., McClure-Begley, A., et al.: Surface and tropospheric ozone trends in the Southern Hemisphere since 1990: possible linkages to poleward expansion of the Hadley circulation, Science Bulletin, 64, 400–409, https://doi.org/10.1016/j.scib.2018.12.021, 2019.

Marais, E. A. and Wiedinmyer, C.: Air quality impact of diffuse and inefficient combustion emissions in Africa (DICE-Africa), Environmental science & technology, 50, 10 739–10 745, https://doi.org/10.1021/acs.est.6b02602, 2016.

Marenco, A., Thouret, V., Nédélec, P., Smit, H., Helten, M., Kley, D., Karcher, F., Simon, P., Law, K., Pyle, J., et al.: Measurement of ozone and water vapor by Airbus in-service aircraft: The MOZAIC airborne program, An overview, Journal of Geophysical Research: Atmospheres, 103, 25 631–25 642, https://doi.org/10.1029/98JD00977, 1998.

Mari, C., Jacob, D. J., and Bechtold, P.: Transport and scavenging of soluble gases in a deep convective cloud, Journal of Geophysical Research: Atmospheres, 105, 22 255–22 267, https://doi.org/10.1029/2000JD900211, 2000.

Mari, C., Cailley, G., Corre, L., Saunois, M., Attié, J., Thouret, V., and Stohl, A.: Tracing biomass burning plumes from the Southern Hemisphere during the AMMA 2006 wet season experiment, Atmospheric Chemistry and Physics, 8, 3951–3961, https://doi.org/10.5194/acp-8-3951-2008, 2008.

McDuffie, E. E., Smith, S. J., O'Rourke, P., Tibrewal, K., Venkataraman, C., Marais, E. A., Zheng, B., Crippa, M., Brauer, M., and Martin, R. V.: A global anthropogenic emission inventory of atmospheric pollutants from sector-and fuel-specific sources (1970–2017): an application of the Community Emissions Data System (CEDS), Earth System Science Data, 12, 3413–3442, https://doi.org/10.5194/essd-12-3413-2020, 2020.

Monks, P. S.: Gas-phase radical chemistry in the troposphere, Chemical Society Reviews, 34, 376–395, https://doi.org/10.1039/B307982C, 2005.

Monks, P. S., Archibald, A., Colette, A., Cooper, O., Coyle, M., Derwent, R., Fowler, D., Granier, C., Law, K. S., Mills, G., et al.: Tropospheric ozone and its precursors from the urban to the global scale from air quality to short-lived climate forcer, Atmospheric Chemistry and Physics, 15, 8889–8973, https://doi.org/10.5194/acp-15-8889-2015, 2015.

Myhre, G., Samset, B. H., Schulz, M., Balkanski, Y., Bauer, S., Berntsen, T. K., Bian, H., Bellouin, N., Chin, M., Diehl, T., et al.: Radiative forcing of the direct aerosol effect from AeroCom Phase II simulations, Atmospheric Chemistry and Physics, 13, 1853–1877, https://doi.org/10.5194/acp-13-1853-2013, 2013.

Naus, S., Domingues, L. G., Krol, M., Luijkx, I. T., Gatti, L. V., Miller, J. B., Gloor, E., Basu, S., Correia, C., Koren, G., et al.: Sixteen years of MOPITT satellite data strongly constrain Amazon CO fire emissions, European Geoscience Union (EGU) General Assembly 2022, pp. 1–25, https://doi.org/10.5194/egusphere-2022-450, 2022.

Nédélec, P., Blot, R., Boulanger, D., Athier, G., Cousin, J.-M., Gautron, B., Petzold, A., Volz-Thomas, A., and Thouret, V.: Instrumentation on commercial aircraft for monitoring the atmospheric composition on a global scale: the IAGOS system, technical overview of ozone and carbon monoxide measurements, Tellus B: Chemical and Physical Meteorology, 67, 27 791, https://doi.org/10.3402/tellusb.v67.27791, 2015.

Pandey, A., Sadavarte, P., Rao, A. B., and Venkataraman, C.: Trends in multi-pollutant emissions from a technology-linked inventory for India: II. Residential, agricultural and informal industry sectors, Atmospheric environment, 99, 341–352, https://doi.org/10.1016/j.atmosenv.2014.09.080, 2014.

Park, M., Randel, W. J., Gettelman, A., Massie, S. T., and Jiang, J. H.: Transport above the Asian summer monsoon anticyclone inferred from Aura Microwave Limb Sounder tracers, Journal of Geophysical Research: Atmospheres, 112, https://doi.org/10.1029/2006JD008294, 2007.

Park, M., Randel, W. J., Emmons, L. K., Bernath, P. F., Walker, K. A., and Boone, C. D.: Chemical isolation in the Asian monsoon anticyclone observed in Atmospheric Chemistry Experiment (ACE-FTS) data, Atmospheric Chemistry and Physics, 8, 757–764, https://doi.org/10.5194/acp-8-757-2008, 2008.

Petetin, H., Thouret, V., Athier, G., Blot, R., Boulanger, D., Cousin, J.-M., Gaudel, A., Nédélec, P., and Cooper, O.: Diurnal cycle of ozone throughout the troposphere over Frankfurt as measured by MOZAIC-IAGOS commercial aircraftDiurnal cycle of ozone throughout the troposphere, Elementa: Science of the Anthropocene, 4, https://doi.org/10.12952/journal.elementa.000129, 2016.

Petetin, H., Jeoffrion, M., Sauvage, B., Athier, G., Blot, R., Boulanger, D., Clark, H., Cousin, J.-M., Gheusi, F., Nedelec, P., et al.: Representativeness of the IAGOS airborne measurements in the lower troposphere, Elementa: Science of the Anthropocene, 6, https://doi.org/10.1525/elementa.280, 2018a.

Petetin, H., Sauvage, B., Parrington, M., Clark, H., Fontaine, A., Athier, G., Blot, R., Boulanger, D., Cousin, J.-M., Nédélec, P., et al.: The role of biomass burning as derived from the tropospheric CO vertical profiles measured by IAGOS aircraft in 2002–2017, Atmospheric Chemistry and Physics, 18, 17 277–17 306, https://doi.org/10.5194/acp-18-17277-2018, 2018b.

Petzold, A., Thouret, V., Gerbig, C., Zahn, A., Brenninkmeijer, C. A., Gallagher, M., Hermann, M., Pontaud, M., Ziereis, H., Boulanger, D., et al.: Global-scale atmosphere monitoring by in-service aircraft–current achievements and future prospects of the European Research Infrastructure IAGOS, Tellus B: Chemical and Physical Meteorology, 67, 28 452, https://doi.org/10.3402/tellusb.v67.28452, 2015.

Pickering, K. E., Thompson, A. M., Tao, W.-K., Rood, R. B., McNamara, D. P., and Molod, A. M.: Vertical transport by convective clouds: Comparisons of three modeling approaches, Geophysical research letters, 22, 1089–1092, https://doi.org/10.1029/95GL00889, 1995.

Reeves, C., Formenti, P., Afif, C., Ancellet, G., Attié, J.-L., Bechara, J., Borbon, A., Cairo, F., Coe, H., Crumeyrolle, S., et al.: Chemical and aerosol characterisation of the troposphere over West Africa during the monsoon period as part of AMMA, Atmospheric Chemistry and Physics, 10, 7575–7601, https://doi.org/10.5194/acp-10-7575-2010, 2010.

Sadavarte, P. and Venkataraman, C.: Trends in multi-pollutant emissions from a technology-linked inventory for India: I. Industry and transport sectors, Atmospheric environment, 99, 353–364, https://doi.org/10.1016/j.atmosenv.2014.09.081, 2014.

Safieddine, S., Boynard, A., Coheur, P.-F., Hurtmans, D., Pfister, G., Quennehen, B., Thomas, J. L., Raut, J.-C., Law, K. S., Klimont, Z., et al.: Summertime tropospheric ozone assessment over the Mediterranean region using the thermal infrared IASI/MetOp sounder and the WRF-Chem model, Atmospheric chemistry and physics, 14, 10 119–10 131, https://doi.org/10.5194/acp-14-10119-2014, 2014.

Safieddine, S., Boynard, A., Hao, N., Huang, F., Wang, L., Ji, D., Barret, B., Ghude, S. D., Coheur, P.-F., Hurtmans, D., et al.: Tropospheric ozone variability during the East Asian summer monsoon as observed by satellite (IASI), aircraft (MOZAIC) and ground stations, Atmospheric Chemistry and Physics, 16, 10 489–10 500, https://doi.org/10.5194/acp-16-10489-2016, 2016.

Sahu, L., Sheel, V., Kajino, M., Gunthe, S. S., Thouret, V., Nedelec, P., and Smit, H. G.: Characteristics of tropospheric ozone variability over an urban site in Southeast Asia: A study based on MOZAIC and MOZART vertical profiles, Journal of Geophysical Research: Atmospheres, 118, 8729–8747, https://doi.org/10.1002/jgrd.50662, 2013.

Sahu, L., Sheel, V., Kajino, M., Deushi, M., Gunthe, S. S., Sinha, P., Sauvage, B., Thouret, V., and Smit, H. G.: Seasonal and interannual variability of tropospheric ozone over an urban site in India: A study based on MOZAIC and CCM vertical profiles over Hyderabad, Journal of Geophysical Research: Atmospheres, 119, 3615–3641, https://doi.org/10.1002/2013JD021215, 2014.

Saunois, M., Reeves, C., Mari, C., Murphy, J., Stewart, D. J., Mills, G., Oram, D., and Purvis, R.: Factors controlling the distribution of ozone in the West African lower troposphere during the AMMA (African Monsoon Multidisciplinary Analysis) wet season campaign, Atmospheric Chemistry and Physics, 9, 6135–6155, https://doi.org/10.5194/acp-9-6135-2009, 2009.

Sauvage, B., Thouret, V., Cammas, J.-P., Gheusi, F., Athier, G., and Nédélec, P.: Tropospheric ozone over Equatorial Africa: regional aspects from the MOZAIC data, Atmospheric Chemistry and Physics, 5, 311–335, https://doi.org/10.5194/acp-5-311-2005, 2005.

Sauvage, B., Thouret, V., Thompson, A., Witte, J., Cammas, J.-P., Nédélec, P., and Athier, G.: Enhanced view of the "tropical Atlantic ozone paradox" and "zonal wave one" from the in situ MOZAIC and SHADOZ data, Journal of Geophysical Research: Atmospheres, 111, https://doi.org/10.1029/2005JD006241, 2006.

Sauvage, B., Gheusi, F., Thouret, V., Cammas, J.-P., Duron, J., Escobar, J., Mari, C., Mascart, P., and Pont, V.: Medium-range mid-tropospheric transport of ozone and precursors over Africa: two numerical case studies in dry and wet seasons, Atmospheric Chemistry and Physics, 7, 5357–5370, https://doi.org/10.5194/acp-7-5357-2007, 2007a.

Sauvage, B., Martin, R., Van Donkelaar, A., Liu, X., Chance, K., Jaeglé, L., Palmer, P., Wu, S., and Fu, T.-M.: Remote sensed and in situ constraints on processes affecting tropical tropospheric ozone, Atmospheric Chemistry and Physics, 7, 815–838, https://doi.org/10.5194/acp-7-815-2007, 2007b.

Sauvage, B., Martin, R. V., Van Donkelaar, A., and Ziemke, J.: Quantification of the factors controlling tropical tropospheric ozone and the South Atlantic maximum, Journal of Geophysical Research: Atmospheres, 112, https://doi.org/10.1029/2006JD008008, 2007c.

Sauvage, B., Thouret, V., Cammas, J.-P., Brioude, J., Nedelec, P., and Mari, C.: Meridional ozone gradients in the African upper troposphere, Geophysical Research Letters, 34, https://doi.org/10.1029/2006GL028542, 2007d.

Sauvage, B., Fontaine, A., Eckhardt, S., Auby, A., Boulanger, D., Petetin, H., Paugam, R., Athier, G., Cousin, J.-M., Darras, S., et al.: Source attribution using FLEXPART and carbon monoxide emission inventories: SOFT-IO version 1.0, Atmospheric Chemistry and Physics, 17, 15 271–15 292, https://doi.org/10.5194/acp-17-15271-2017, 2017.

Sheel, V., Sahu, L., Kajino, M., Deushi, M., Stein, O., and Nedelec, P.: Seasonal and interannual variability of carbon monoxide based on MOZAIC observations, MACC reanalysis, and model simulations over an urban site in India, Journal of Geophysical Research: Atmospheres, 119, 9123–9141, https://doi.org/10.1002/2013JD021425, 2014.

Singh, H., Herlth, D., Kolyer, R., Chatfield, R., Viezee, W., Salas, L., Chen, Y., Bradshaw, J., Sandholm, S., Talbot, R., et al.: Impact of biomass burning emissions on the composition of the South Atlantic troposphere: Reactive nitrogen and ozone, Journal of Geophysical Research: Atmospheres, 101, 24 203–24 219, https://doi.org/10.1029/96JD01018, 1996.

Stein, O., Schultz, M. G., Bouarar, I., Clark, H., Huijnen, V., Gaudel, A., George, M., and Clerbaux, C.: On the wintertime low bias of Northern Hemisphere carbon monoxide found in global model simulations, Atmospheric chemistry and physics, 14, 9295–9316, https://doi.org/10.5194/acp-14-9295-2014, 2014.

Stevenson, D., Young, P., Naik, V., Lamarque, J.-F., Shindell, D. T., Voulgarakis, A., Skeie, R. B., Dalsoren, S. B., Myhre, G., Berntsen, T. K., et al.: Tropospheric ozone changes, radiative forcing and attribution to emissions in the Atmospheric Chemistry and Climate Model Intercomparison Project (ACCMIP), Atmospheric Chemistry and Physics, 13, 3063–3085, https://doi.org/10.5194/acp-13-3063-2013, 2013.

Stohl, A., Bonasoni, P., Cristofanelli, P., Collins, W., Feichter, J., Frank, A., Forster, C., Gerasopoulos, E., Gäggeler, H., James, P., et al.: Stratosphere-troposphere exchange: A review, and what we have learned from STACCATO, Journal of Geophysical Research: Atmospheres, 108, https://doi.org/10.1029/2002JD002490, 2003.

Tang, Q., Prather, M., and Hsu, J.: Stratosphere-troposphere exchange ozone flux related to deep convection, Geophysical Research Letters, 38, https://doi.org/10.1029/2010GL046039, 2011.

Tarasick, D., Carey-Smith, T., Hocking, W., Moeini, O., He, H., Liu, J., Osman, M., Thompson, A., Johnson, B., Oltmans, S., et al.: Quantifying stratosphere-troposphere transport of ozone using balloon-borne ozonesondes, radar windprofilers and trajectory models, Atmospheric Environment, 198, 496–509, https://doi.org/10.1016/j.atmosenv.2018.10.040, 2019.

Thompson, A. M., Witte, J. C., Hudson, R. D., Guo, H., Herman, J. R., and Fujiwara, M.: Tropical tropospheric ozone and biomass burning, Science, 291, 2128–2132, https://doi.org/10.1126/science.291.5511.2128, 2001.

Thompson, A. M., Witte, J. C., McPeters, R. D., Oltmans, S. J., Schmidlin, F. J., Logan, J. A., Fujiwara, M., Kirchhoff, V. W., Posny, F., Coetzee, G. J., et al.: Southern hemisphere additional Ozonesondes (SHADOZ) 1998–2000 tropical ozone climatology 1. Comparison with Total ozone mapping spectrometer (TOMS) and ground-based measurements, Journal of Geophysical Research: Atmospheres, 108, https://doi.org/10.1029/2001JD000967, 2003a.

Thompson, A. M., Witte, J. C., Oltmans, S. J., Schmidlin, F. J., Logan, J. A., Fujiwara, M., Kirchhoff, V. W., Posny, F., Coetzee, G. J., Hoegger, B., et al.: Southern Hemisphere Additional Ozonesondes (SHADOZ) 1998–2000 tropical ozone climatology 2. Tropospheric variability and the zonal wave-one, Journal of Geophysical Research: Atmospheres, 108, https://doi.org/10.1029/2002JD002241, 2003b.

Thompson, A. M., Stauffer, R. M., Wargan, K., Witte, J. C., Kollonige, D. E., and Ziemke, J. R.: Regional and Seasonal trends in tropical ozone from SHADOZ profiles: Reference for models and satellite products, Journal of Geophysical Research: Atmospheres, 126, e2021JD034 691, https://doi.org/10.1029/2021JD034691, 2021.

Thouret, V., Clark, H., Petzold, A., Nédélec, P., and Zahn., A.: IAGOS: Monitoring Atmospheric Composition for Air Quality and Climate by Passenger Aircraft, pp. 1–14, Singapore: Springer Nature Singapore, https://doi.org/https://doi.org/10.1007/978-981-15-2527-8_57-1, 2022.

van der A, R. J., Mijling, B., Ding, J., Koukouli, M. E., Liu, F., Li, Q., Mao, H., and Theys, N.: Cleaning up the air: effectiveness of air quality policy for SO 2 and NO x emissions in China, Atmospheric Chemistry and Physics, 17, 1775–1789, https://doi.org/10.5194/acp-17-1775-2017, 2017.

van der Werf, G. R., Randerson, J. T., Giglio, L., Collatz, G. J., Kasibhatla, P. S., and Arellano Jr, A. F.: Interannual variability in global biomass burning emissions from 1997 to 2004, Atmospheric Chemistry and Physics, 6, 3423–3441, https://doi.org/doi.org/10.5194/acp-6-3423-2006, 2006.

Van der Werf, G. R., Randerson, J. T., Giglio, L., Collatz, G., Mu, M., Kasibhatla, P. S., Morton, D. C., DeFries, R., Jin, Y. v., and van Leeuwen, T. T.: Global fire emissions and the contribution of deforestation, savanna, forest, agricultural, and peat fires (1997–2009), Atmospheric chemistry and physics, 10, 11 707–11 735, https://doi.org/10.5194/acp-10-11707-2010, 2010.

Wang, T., Xue, L., Brimblecombe, P., Lam, Y. F., Li, L., and Zhang, L.: Ozone pollution in China: A review of concentrations, meteorological influences, chemical precursors, and effects, Science of the Total Environment, 575, 1582–1596, https://doi.org/10.1016/j.scitotenv.2016.10.081, 2017.

Wild, O., Pochanart, P., and Akimoto, H.: Trans-Eurasian transport of ozone and its precursors, Journal of Geophysical Research: Atmospheres, 109, https://doi.org/10.1029/2003JD004501, 2004.

Yamasoe, M. A., Sauvage, B., Thouret, V., Nédélec, P., Le Flochmoen, E., and Barret, B.: Analysis of tropospheric ozone and carbon monoxide profiles over South America based on MOZAIC/IAGOS database and model simulations, Tellus B: Chemical and Physical Meteorology, 67, 27 884, https://doi.org/10.3402/tellusb.v67.27884, 2015.

Yarragunta, Y., Srivastava, S., Mitra, D., Le Flochmoën, E., Barret, B., Kumar, P., and Chandola, H.: Source attribution of carbon monoxide and ozone over the Indian subcontinent using MOZART-4 chemistry transport model, Atmospheric Research, 227, 165–177, https://doi.org/10.1016/j.atmosres.2019.04.019, 2019.

Zhang, Y., Cooper, O. R., Gaudel, A., Thompson, A. M., Nédélec, P., Ogino, S.-Y., and West, J. J.: Tropospheric ozone change from 1980 to 2010 dominated by equatorward redistribution of emissions, Nature Geoscience, 9, 875–879, https://doi.org/10.1038/ngeo2827, 2016.

Zhang, Y., West, J. J., Emmons, L. K., Flemming, J., Jonson, J. E., Lund, M. T., Sekiya, T., Sudo, K., Gaudel, A., Chang, K.-L., et al.: Contributions of world regions to the global tropospheric ozone burden change from 1980 to 2010, Geophysical Research Letters, 48, e2020GL089 184, https://doi.org/10.1029/2020GL089184, 2021.

Zheng, B., Chevallier, F., Ciais, P., Yin, Y., Deeter, M. N., Worden, H. M., Wang, Y., Zhang, Q., and He, K.: Rapid decline in carbon monoxide emissions and export from East Asia between years 2005 and 2016, Environmental Research Letters, 13, 044 007, https://doi.org/10.1088/1748-9326/aab2b3, 2018a.

Zheng, B., Chevallier, F., Ciais, P., Yin, Y., and Wang, Y.: On the role of the flaming to smoldering transition in the seasonal cycle of African fire emissions, Geophysical Research Letters, 45, 11–998, https://doi.org/10.1029/2018GL079092, 2018b.

Zheng, B., Chevallier, F., Yin, Y., Ciais, P., Fortems-Cheiney, A., Deeter, M. N., Parker, R. J., Wang, Y., Worden, H. M., and Zhao, Y.: Global atmospheric carbon monoxide budget 2000–2017 inferred from multi-species atmospheric inversions, Earth System Science Data, 11, 1411–1436, https://doi.org/10.5194/essd-11-1411-2019, 2019.

Ziemke, J., Chandra, S., Duncan, B., Schoeberl, M., Torres, O., Damon, M., and Bhartia, P.: Recent biomass burning in the tropics and related changes in tropospheric ozone, Geophysical Research Letters, 36, https://doi.org/10.1029/2009GL039303, 2009.

Ziemke, J. R., Oman, L. D., Strode, S. A., Douglass, A. R., Olsen, M. A., McPeters, R. D., Bhartia, P. K., Froidevaux, L., Labow, G. J., Witte, J. C., et al.: Trends in global tropospheric ozone inferred from a composite record of TOMS/OMI/MLS/OMPS satellite measurements and the MERRA-2 GMI simulation, Atmospheric Chemistry and Physics, 19, 3257–3269, https://doi.org/10.5194/acp-19-3257-2019, 2019.